



Scientific Design of Multilayer Fog Collectors

Dissertation Thesis

Study programme:
Study branch:

P3106 Textile Engineering
Textile Technics and Materials Engineering

Author:
Thesis Supervisor:

Musaddaq Azeem, M.Sc.
prof. Ing. Jakub Wiener, Ph.D.
Department of material engineering



Declaration

I hereby certify, I, myself, have written my dissertation as an original and primary work using the literature listed below and consulting it with my thesis supervisor and my thesis counsellor.

I acknowledge that my dissertation is fully governed by Act No. 121/2000 Coll., the Copyright Act, in particular Article 60 – SchoolWork.

I acknowledge that the Technical University of Liberec does not infringe my copyrights by using my dissertation for internal purposes of the Technical University of Liberec.

I am aware of my obligation to inform the Technical University of Liberec on having used or granted license to use the results of my dissertation; in such a case the Technical University of Liberec may require reimbursement of the costs incurred for creating the result up to their actual amount.

At the same time, I honestly declare that the text of the printed version of my dissertation is identical with the text of the electronic version uploaded into the IS/STAG.

I acknowledge that the Technical University of Liberec will make my dissertation public in accordance with paragraph 47b of Act No. 111/1998 Coll., on Higher Education Institutions and on Amendment to Other Acts (the Higher Education Act), as amended.

I am aware of the consequences which may under the Higher Education Act result from a breach of this declaration.

October 4, 2021

Musaddaq Azeem, M.Sc.

Dedication

I dedicate this thesis to my wife Arshia Azeem

Acknowledgement

I set my unfeigned and meek thanks before Almighty Allah, who created the universe and bestowed mankind with knowledge and wisdom.

First of all, I am thankful to my PhD supervisor **prof. Ing. Jakub Wiener**, who despite his busiest routine work, provided his dexterous guidance and valuable suggestions throughout this research effort.

I also deem my deep feelings of regard and gratitude to **prof. Dr. Jacques Dumais** (Adolfo Ibáñez University - Campus Viña del Mar, Chile) providing me the platform and technical help for research work. I do not have words at my command to express his kindness and humble cooperation during the research work.

Thanks are extended to the professors of the Technical University of Liberec, Dean, Vice Dean of Faculty of Textile Engineering, the Department of Material Engineering, where I was able to study the new technologies, innovations, and research ideas.

I would like to acknowledge Prof. Ing. Jiří Militký, CSc., doc. Ing. Antonin Havelka and Prof. Ing. Lubos Hes, DrSc. whose expertise was quite helpful in formulating the research work

I am also very grateful to Ing. Blanka Tomkova, Ph.D. (HOD, Department of Materials Engineering) for her special assistant regarding funds for internships and conferences. I am really thankful to Ing. Bohumila Keilová, and Ing. Hana Musilová for their help and support.

I would particularly like to say a special thanks to Prof. Dr. Morikawa Hideaki (Shinshu University, Japan) and Prof. Dr. Nicolas Javier Alvarez (Drexel University, PA, USA) for inviting me to their labs for the internship.

My gratitude will remain deficient if I do not name the contribution of my most sincere friends Dr. M. Tayyab Noman, Dr. Zuhaib Ahmad, Dr. M. Zaman Khan, and Dr. Faisal Siddique who assisted me in data collection and experimental work. I am a little thankful to Dr. Azam Ali who didn't acknowledge me in his thesis.

Finally, I would like to thank my mother, wife, daughter, son, and brother for their encouragement, and prayers to complete this dissertation.

Musaddaq Azeem

Table of Contents

ABSTRACT.....	v
ABSTRAKT	vi
Nomenclature.....	vii
Greek	vii
Abbreviation.....	vii
Sub indices	viii
List of Figures	ix
List of Tables	xii
1. Introduction	1
2. Purpose and Aim of the Study.....	3
3. Literature Review.....	5
3.1. Water scarcity.....	5
3.2. Alternative water resources.....	5
3.3. Fog Collectors	6
3.3.1. Standard fog collector (SFC).....	9
3.3.2. <i>Large fog collector (LFC)</i>	10
3.4. Fundamentals of Fog Collection	11
3.5. Multilayer Fog Collectors	11
3.6. Wettability of Fog Collectors.....	12
3.7. Quality of Fog Water.....	15
4. Theory.....	17
4.1. Total Water Collection Efficiency (η_{tot})	17
4.2. Maximizing η_{tot}	21

4.3.	Fluid Mechanics Prediction of A_{∞} / A	23
4.4.	Models for Filtered Fraction	25
4.4.1.	Glauert 1932 Model.....	25
4.4.2.	Rivera 2011 Model	26
4.4.3.	Koo1973 Model	27
5.	Research Methodology	28
5.1.	Materials.....	28
5.2.	Collector Design.....	29
5.2.1.	Construction of prototypes	29
5.3.	Measurement of Aerodynamic Collection Efficiency.....	31
5.3.1	Yield measurements.....	33
5.4.	Wettability.....	34
5.4.1.	Plasma treatment with DBD reactor	34
5.4.2.	Silane treatment	35
5.4.3.	Characterization.....	35
5.4.4.	Fog generator	35
6.	Results and Discussion	37
6.1.	Optimal Design of Multilayer Fog Collectors.....	37
6.1.1.	Efficiency of multilayer fog collector	39
5.2.	Wettability of Vertical Harps for Fog Collection.....	52
6.2.1.	Characterization.....	54
7.	Conclusions and Future Work	61
8.	References	63
9.	List of publications by the author	74
9.1.	Publications in journals	74

9.2. International Conferences	75
9.3. Citations	76
Curriculum Vitae	77

ABSTRACT

The growing concerns over desertification have spurred research into technologies aimed at acquiring water from nontraditional sources such as dew, fog, and water vapor. Some of the most promising developments have focused on improving designs to collect water from fog. However, the absence of a shared framework to predict, measure, and compare the water collection efficiencies of new prototypes is becoming a major obstacle to progress in the field. We addressed this problem by providing a general theory to design efficient fog collectors as well as a concrete experimental protocol to furnish our theory with all the necessary parameters to quantify the effective water collection efficiency. We showed in particular that multilayer collectors are required for high fog collection efficiency and that all efficient designs are found within a narrow range of mesh porosity. We support our conclusions with measurements on simple multilayer harp collectors.

Surface wettability contributed a major role in fog harvesting. Hydrophilic surfaces offer fast nucleation, while hydrophobic surfaces provide the droplets rapid transportation. Many animals and plants in arid environments control this tradeoff by naturally coated biphilic surfaces with structural designed wettability. This patterned wettability gives a high affinity for fog collection. This mechanism aims to reduce the friction and pinning force of the fog droplets sliding down towards storage. The reason to replace the traditional Raschel mesh with a harp design is to capture the maximal fog by avoiding clogging. We also established an experimental part focus on the wettability (hydrophilicity and hydrophobicity) of vertical harp or fog collector element (FCE). The FCE treated with hydrophilic treatments exhibited adverse effects while hydrophobic coating slightly improved the collection rate. Moreover, we examined the contact angle hysteresis (CAH) of our prototypes to verify the wettability effect.

KEYWORDS: fluid mechanics, fog collector, harp design, porous media, water collection efficiency, hydrophilicity, hydrophobicity, fog harvesting, fog collector element

ABSTRAKT

Rostoucí obavy z rozšiřování pouští podnítily výzkum technologií zaměřených na získávání vody z netradičních zdrojů, jako je rosa, mlha a vodní pára. Některé z nejslibnějších projektů se zaměřují na zdokonalení konstrukcí pro získávání vody z mlhy. Hlavní překážkou pokroku v této oblasti se však stává neexistence společného rámce pro předvídání, měření a porovnávání účinnosti sběru vody u nových prototypů. Tento problém jsme řešili tím, že jsme navrhli obecnou teorii pro projektování účinných sběračů mlhy a také konkrétní experiment, který naši teorii vybavil všemi potřebnými parametry pro kvantifikaci efektivní účinnosti sběru vody. Ukázali jsme zejména, že pro vysokou účinnost sběru mlhy jsou nutné vícevrstvé kolektory a že všechny účinné konstrukce se nacházejí v úzkém rozmezí pórovitosti sítě. Naše závěry jsme podpořili měřeními na jednoduchých vícevrstvých harfových kolektorech.

Smáčivost povrchu hraje při sběru mlhy významnou roli. Hydrofilní povrchy nabízejí rychlou nukleaci, zatímco hydrofobní povrchy zajišťují rychlý transport kapek. Mnoho živočichů a rostlin v suchých prostředích tento kompromis řídí přirozeným pokrytím bifilních povrchů se strukturálně řízenou smáčivostí. Tato lokální smáčivost poskytuje vysokou afinitu ke sběru mlhy. Tento mechanismus má za cíl usnadnit transport kapiček mlhy klouzajících dolů směrem k úložišti. Důvodem nahrazení tradiční rašlové sítě harfovou konstrukcí je zachycení maximálního množství mlhy zamezením jejího „ucpávání“ vodou. Experimentálně byla realizována i část zaměřená na smáčivost (hydrofilnost a hydrofobnost) vertikální harfové struktury nebo mlhového sběrného prvku (FCE). Modifikace FCE hydrofilní úpravou vykazovalo zhoršený záchyt vody, zatímco hydrofobní úprava tento záchyt mírně zlepšila. Kromě toho jsme zkoumali hysterezi kontaktního úhlu (CAH) našich prototypů, abychom plně kvantifikovali smáčivost povrchu kolektoru.

KLÍČOVÁ SLOVA: mechanika tekutin, mlhový kolektor, harfová struktura, porézní médium, účinnost sběru vody, hydrofilnost, hydrofobnost, sběr mlhy, prvek mlhového kolektoru.

Nomenclature

A	Frontal area of the collector
A_∞	Area of unperturbed incoming fog flow
C_D	Drag coefficient
d	Diameter of the thread
d_∞	Span of streamlines whose droplets will be intercepted by the thread
F_D	Drag force
J	Water flux or yield
k	Pressure drop coefficient
N	Number of layers
ΔP	Pressure drop
Re	Reynolds number
l	length
s	Solidity or solid fraction or shade coefficient (used in previous studies)
Stk	Stokes number
u	velocity of the air stream
u_∞	Velocity of the unperturbed fog flow
χ	Incident fraction
F_g	Force of gravity
F_d	Driving force
η	Efficiency

Greek

ν	Kinematic viscosity
φ	Filtered fraction
μ	Dynamic viscosity
ρ	Density

Abbreviation

ACE	Aerodynamic collection efficiency
-----	-----------------------------------

LWC	Liquid water content
max	Maximum
RHS	Right hand side
Eq.	Equation
FCE	Fog collector element
PES	Polyester
PE	Polyethylene
PP	Polypropylene
WCA	Water contact angle
CAH	Contact angle hysteresis
AFM	Atomic force microscope
DBD	Dielectric barrier discharge
LWF	Liquid water flux
SFC	Standard fog collector
LFC	large fog collector

Sub indices

tot	Total
capt	Capture
drain	Drainage
AC	Aerodynamic Collection
obs	Observed
pred	Predicted
opt	Optimal
a	Advancing
r	Receding

List of Figures

Figure 1: Aerodynamics of fog collection. (A) A stand of the bromeliad <i>Tillandsia landbeckii</i> in the Atacama Desert of Chile. (B) Close-up of <i>Tillandsia landbeckii</i> showing the dense three-dimensional array of leaves. Inset: the hydrophilic scale-like trichomes covering the leaves and branches of <i>Tillandsia</i>	4
Figure 2: world map indicates the spots where fog collection has been carried out	7
Figure 3: Fog collections with SFC and LFC in the different regions of the world	8
Figure 4: Fog Collectors, (A) SFC (B) (LFC)	10
Figure 5: Wind speed is plotted against the efficiency and the LWC. LWC and wind velocity maximize the efficiency of the fog collector	11
Figure 6: (A) Prototype of a 1 m × 1 m multiharp fog collector with a mesh solidity $s = 0.3$ per layer and $N = 4$ layers. (B) Top view of the air flow around a fog collector. The typical collector length is $1\text{m} \leq l \leq 10\text{m}$. Streamlines are drawn based on wind tunnel experiments by Ito and Garry [101], with square mesh gauze of solidity 0.63 at $Re \approx 10^6$ based on the collector size. (C) Close-up of the air flow around the section of two cylindrical threads of the collector. The diameter of the threads $d \approx 150 - 160 \mu\text{m}$ for the collector is shown in (B) and the experiments discussed below. $d_\alpha(r)$ represents the span of streamlines whose droplets will be intercepted by the thread directly downstream. The top and bottom halves of the diagram show the interception of the small and large droplets, respectively; dashed lines indicate approximate trajectories of intercepted droplets. Streamlines are based on Gordon’s simulations [102] at $Re = 20$ based on the thread diameter.....	18
Figure 7: Knitting pattern Raschel mesh. (A) Prototype 100 mm×100 mm. (B) Structure of mesh	29
Figure 8: Harp collector built with PE monofilament. (A) Prototype 100 mm × 100 mm. (B) microscopic view of PE monofilament.....	30
Figure 9: Construction of harp collector with evenly spaced notches	31
Figure 10: Flow diagram of the platforms to quantify the two stages of fog droplet collection ..	32
Figure 11: Wind tunnel platform used to measure the large scale flow field	33

Figure 12: Measurement of the yield. (A) The prototypes from the opening of a wind tunnel. (B) Optimized the distance between wind tunnel and prototype	34
Figure 13: The diagram of the experimental setup for fog collection	36
Figure 14: Yield collected of four different collector elements after 15 minutes with one layer.	37
Figure 15: (A) Multilayer arrangement comparison. (B) In-line arrangements of layers. (C) Stagger arrangements of layers	38
Figure 16: Effect of interlayer spacing on the yield of multilayer collectors	39
Figure 17: Aerodynamic collection efficiency for multi-layer fog collectors. (A) Filtered fraction predicted from the Steiros2018 model (Eqs. 12-14). (B) The incident fraction computed from geometrical considerations (Eq. 8, second term on the RHS)	41
Figure 18: The ACE Ridge - a 3D representation of ACE as a function of the two control parameters s and N . A maximum ACE of 0.49 is observed for 10 layers, each with an operating solidity of 0.17. Single-layer collectors are confined to the line $N = 1$ and have an ACE below 0.3. (Note: we have treated N as a continuous variable for illustration).....	42
Figure 19: The maximal ACE as a function of N (plotted on a log scale). Although $\max(\eta_{AC})$ increases with increasing N , the relative ACE increase, $\Delta\max(\eta_{AC})/\max(\eta_{AC})$, becomes small for $N > 5$ and negligible for $N > 10$	43
Figure 20: The ACE ridge of four alternative models for the filtered fraction. (A) The filtered fraction of the various models. Note the model-dependent form of the asymptotic behavior of $\varphi(s)$ as $s \rightarrow 0$. (B) Design space for the models listed in A. The blue subspace marks the region within which ACE is locally maximized, either at constant N (lower edge of the blue strip) or at constant s (upper edge of the blue strip). The red square is the suggested target design	46
Figure 21: The $\max(\eta_{AC})$ subspace (blue curves) overlaps closely with level curves for the filtered fraction (red) in design space	46
Figure 22: Measurement of ACE for a multi-layer harp collector ($s = 0.17$, $N = 4$). (A) Close-up of the fog jet filtering through a closed collector. (B) Close-up of the fog jet filtering through a 4-layer collector. (C) Close-up of the fog jet filtering through an open collector. (E) Fog flows around a closed collector. (E), a 4-layer harp (F), and an open frame. The blue curves indicate streamlines	47

Figure 23: Operational shade coefficient of a simple harp (A) Photo of the mesh under operating conditions. (B) Binary (black/white) version of (A) Used to compute the solidity. The “dry” solidity is 0.075 while the “wet” solidity is 0.17 48

Figure 24: Close-up of the fog jet filtering through the collector with the key variables characterizing the flow field indicated..... 50

Figure 25: Proposed standard for the measurement of ACE. Prototypes should be square with 100 mm ×100 mm of open area and a frame of 5 mm on all sides. The operational solid fraction s and the number of layers N are free parameters to be adjusted. The ACE should be measured at a free stream velocity close to $5 \text{ m}\cdot\text{s}^{-1}$ and in the presence of fog 51

Figure 26: Yield measurements. (A) The yield of multi-layer harps ($1 \leq N \leq 10$, $s = 0.17$, inter-layer spacing of 6 mm) compared to two plies of Raschel mesh with $s = 0.7$ at a fog velocity $u_\infty = 4 \text{ m}\cdot\text{sec}^{-1}$ (B) Field measurements of yield over 20 days 52

Figure 27: Contact angle results of untreated, hydrophilic surfaces and hydrophobic surfaces... 54

Figure 28: Water collection yield for single monofilament of all three samples..... 55

Figure 29: Display the position and shape of water droplets on the samples. (a) Illustration of fog on the untreated filament before slide down. (b) Demonstration of captured droplet areas of hydrophilic filament in the same length segment as an original filament with droplet area. (c) A bunch of small fog droplets adsorbs on the hydrophobic surface before it starts to roll down. (d) Driving force (F_d) produces a wettability slope of droplets on the surface of vertical FCEs dealt with plasma treatment. (e) The fog droplets grown on the hydrophobic surface approach the significant sliding volume and rapidly move along the vertical path with the force of gravity (F_g) 56

Figure 30: AFM images of (a) untreated and (b) dry air plasma treated PE monofilament samples 57

Figure 31: Deposition and adhesion of droplets to the monofilament. In (a), hydrophilic surface bond with droplet and provide enough time to make it bigger until it forces of gravity overcomes the weight of the droplet. In (b), the hydrophobic surface does not allow the droplets to be stayed there for a longer time and compel the droplets to roll down 58

Figure 32: A water droplet on a vertical surface of fog collector element, caught at the critical advancing angle (θ_a) and the critical receding angle (θ_r). 59

Figure 33: Droplets impaction on the fog collector element 60

List of Tables

Table 1: Specification of all the materials used for the study	28
Table 2: Properties of TWIN-humidifier	36
Table 3: The filtered fraction, φ , computed as a ratio of areas (l_{∞}^2/l^2).....	49

1. Introduction

Many regions of the world experience chronic water shortages and the associated impacts on human health and economic growth [1]. This crisis has spurred research for novel technologies to exploit alternative water sources such as fog [2, 3], dew [4-6], and even water vapor [7], where the conditions are favorable, fog stands out as one of the most attractive water sources because fog water can be collected in large amounts without any input of energy [8-10]. Because of its appeal, fog collection has been studied intensively in recent years resulting in a large body of work focused on improving the efficiency of fog collectors [11-18]. Fog collection is usually achieved with fine meshes exposed to the incoming fog stream. The minuscule fog droplets intercepted by the threads accumulate until they reach a critical size at which point the force of gravity overcomes the surface tension forces and allows the drop to slide down the collector's surface to reach the gutter at its base.

The central design challenge for efficient fog collection is to accommodate two physical processes that have opposite requirements [19]. On the one hand, fog collecting meshes cannot be very dense or present a major obstacle to the flow of air otherwise the incoming fog stream will simply bypass the structure laterally. On the other hand, fog droplets can be intercepted only if they encounter a mesh element while they transit through the collector. Therefore, overly open meshes are poor collectors, just as meshes are too dense. A related issue for fog collectors is clogging of the mesh by the water droplets that have been captured thus making the collector less permeable to the incoming fog and reducing the overall water collection efficiency [11].

Material scientists have sought to alleviate the problem of clogging by making structural changes to the mesh such as using harp designs [17, 20] or hierarchical branched patterns [21, 22] instead of using the standard criss-crossing meshes that tend to hold water drops in place. Other material science contributions have explored modifications of the collecting surfaces to allow intercepted droplets to coalesce and move quickly under the action of gravity [23-25]. In particular, modifications of the contact angle hysteresis can reduce the critical size a drop needs to reach before it is freed from the mesh [11]. However, many of these possible improvements

will have to be scaled to realistic sizes ($>1 \text{ m}^2$) and produced at a competitive price (less than USD 25 per m^2) [26] before they can be used in the field.

2. Purpose and Aim of the Study

The supply of pure water has become a social issue and it obliges the material scientists working mutually with functional ecological entities to bring novel fog collection techniques. An alternative avenue to improve the performance of fog collectors arises from observations of the bromeliad *Tillandsia landbeckii*, a plant that relies almost exclusively on fog to fulfill its water needs [27-29]. *Tillandsia* forms large stands on the fog-prone coast of the Atacama Desert of Chile. These stands are striking in that the plants self-organize into bands orthogonal to the flow of fog (Figure 1A), thus allowing each plant direct access to the fog stream. Moreover, the leaves and stems of *Tillandsia* are reduced to thin filamentous structures organized into a three-dimensional mesh, a unique feature among bromeliads (Figure 1B).

Finally, a dense layer of hydrophilic trichomes covers the plant surfaces (Figure 1B). Three length scales emerge from observations of *Tillandsia*: the smallest length scale is that of the trichomes ($\sim 100 \mu\text{m}$) involved in intercepting fog droplets, the intermediate length scale is the characteristic pore size between the leaves ($\sim 1 \text{ mm}$) through which the fog stream must filter, the largest length scale is the self-organization of *Tillandsia* plants into fog collecting stands ($\geq 1 \text{ m}$). These observations indicate that 3-D structures, with appropriately selected length scales, can be efficient at collecting fog.

Inspired by *Tillandsia landbeckii*, we investigated the potential offered by multilayer designs for improving the water collection efficiency of fog collectors (Figure 6A-C). Such 3-D structures can resolve many of the issues associated with single-layer collectors, including clogging. Despite having been field-tested more than 50 years ago; [30] the performance of multilayer collectors have not been studied theoretically except for one recent study [31]. Specifically, it is still unclear whether broadly applicable design principles exist. Here, we formalize the fundamental tradeoff associated with the capture of fog with multilayer collectors and demonstrate that simple design rules can guarantee nearly optimal fog collection efficiency.

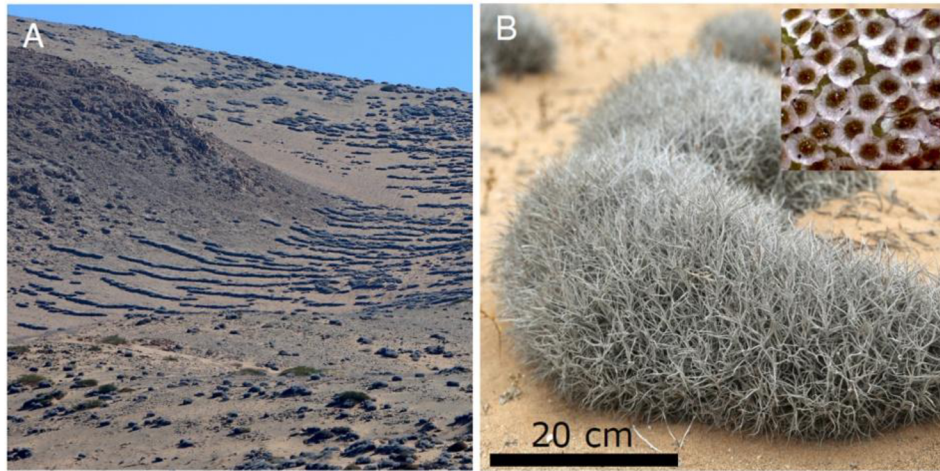


Figure 1: Aerodynamics of fog collection. (A) A stand of the bromeliad *Tillandsia landbeckii* in the Atacama Desert of Chile. (B) Close-up of *Tillandsia landbeckii* showing the dense three-dimensional array of leaves. Inset: the hydrophilic scale-like trichomes covering the leaves and branches of *Tillandsia*.

Ideally, the most favorable fog collector would harvest the maximum fog droplets to accomplish. Our objective in this study is to prove that the total efficiency of our fog collector relies on the design and geometry of the collector. Although, hydrophobicity also plays an important role to enhance the efficiency of fog collectors. The tiny droplets of fog are deposited on the surface of the collector element and enlarge by coalesces of the neighboring droplets with an elongated shape. Thus the fusion of enlarged water droplets triggered a minute slide along with the collector element. Meanwhile, the gap is available for new incoming fog droplets to be deposited on the collector elements and fill the surface with large droplets. While sliding downward, all the droplets have been rolled down on their way towards the storage. The whole phenomenon from the birth of droplets to slipping down depends upon the surface repellent structure and design of the collector. These parameters lead to confirm that the design of geometry in addition to hydrophobicity is the most important variable to enhance efficiency even expose to severe environmental conditions. However, CAH mimics a vital role in the coating phenomena to predict the significance of applied material.

3. Literature Review

Water is one of the most abundant and valuable compounds on earth and is considered a major renewable energy resource for mankind and living organisms. Due to water scarcity, there is a dire need for harvesting water from all of its available resources. Fog is one of those water resources, and it is widely considered as one of the most economical and facile methods in arid agricultural regions where clean and pure water is a necessity for drinking as well as being required for farming purposes.

3.1. Water Scarcity

However, human beings are using only an insignificant portion ($< 0.36\%$) of clean and pure water for drinking and irrigation purposes [1]. Indeed, 66% of the total population of the world is facing water shortage [32]. Therefore, over 1 billion people in the world are not able to drink clean water. Sunrise each morning signs the visibility of water everywhere, even in arid places. According to a U.N.'s 2012, African women spend 40 billion hours a year, fetching water. The scarcity of clean water has become an alarming situation and to overcome this global issue, alternative water resources i.e., fog [2, 3], rain [33], dew [4, 6], etc., have gained considerable attention from researchers and scientists to fill up the need of freshwater.

3.2. Alternative Water Resources

Fog or humidity in the air condenses onto the surfaces of leaves in the form of dew, if collected in large quantities, may act as a source of potable water supplementing the need of community living in dried regions [19, 34]. There are several projects on six continents (North and South America, Europe, Africa, Asia, and Australia) to harvest fog water [19, 34-38], among which a few are more successful than others. (ADD EXP) Since 1998, a worldwide conference on fog and dew harvesting organized tri-annual (<http://www.fogquest.org/conference.html>), bringing the scientists and scientific conclusions onto one platform with new techniques.

Fog is one of the extensively used alternative water resources that provide clean and dirt-free water. Fog harvesting is an innovative approach for water collection that has gained tremendous attention in recent years [9, 39]. Several studies have shown that in arid and semi-arid regions, fog plays a vital role in the fulfillment of water, considering the deficiency of it in these regions. From time to time, researchers have been proposing different and versatile methods around fog harvesting [9, 40-42] on the lab scale and commercial level. Similarly, the Atacama Desert in Chile is one of the driest spots in the world that is rarely recorded to have rain, but fog coming from the sea or ocean could become the alternative source of freshwater.

3.3. Fog Collectors

Most of the studies used the Raschel mesh (produced in Chile) globally. The interlacing is made of vertically stretched triangles to help rapid run-off of the water. For the last two decades, the double-layered mesh is being used to collect the fog water because it gets a higher water yield [10, 11, 14, 16, 23, 31, 34, 43-46]. Figure 2 points out the places in the world where fog harvesting has been studied (<http://www.fogquest.org/>).

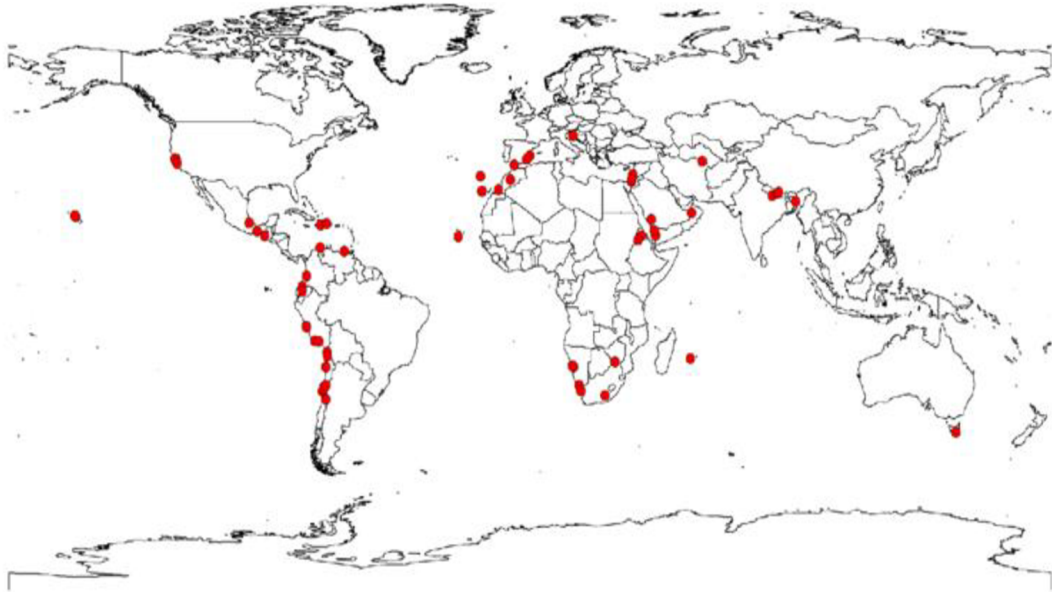


Figure 2: world map indicates the spots where fog collection has been carried out

The role of Raschel mesh is as common as a portable water collector, and it is considered as a standard material when dealing or working with fog harvesting and condensation. Now in this review literature, we discussed some other types of meshes and elaborated on their efficiencies as well as propose a comparison with the standard raschel mesh. In an experimental study, Tan *et al.* prepared and used polyethylene mesh as a novel water collector and made a comparison with raschel mesh for their water harvesting efficiency. They explained that the durability and elastic recovery of polyethylene mesh are much higher than raschel mesh as it could withstand strong wind [47].

Different fog collection yield is reported accordingly, Namibia [48], Jordan [49], Croatia [50], Yemen [51], Guatemala [52], South Africa [53], Oman [41, 54-56], Peru [57], Ecuador [58], Morocco [59], Canary Islands [59, 60], Saudi Arabia [61], Chile [62], while a site in Oman [54] exhibited the highest fog water collection rate as shown in figure 3.

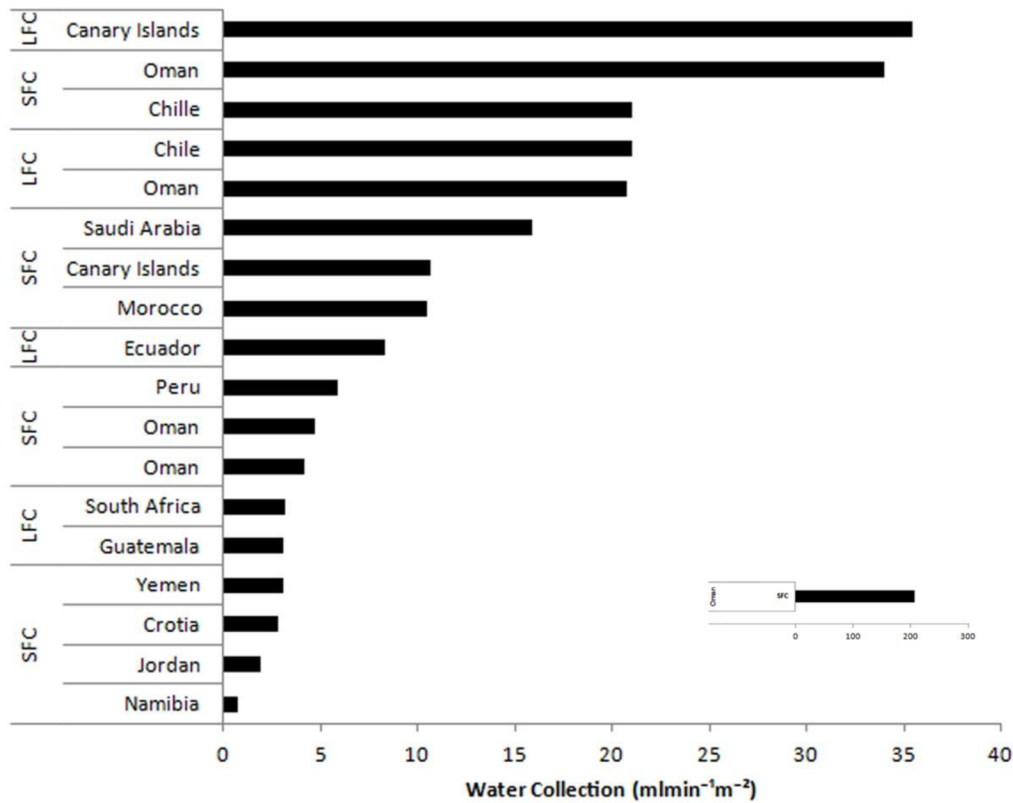


Figure 3: Fog collections with SFC and LFC in the different regions of the world

It was also further explored how the water collection yield rate depends on the geometry and wettability of these structures therefore many scientists made changes in the design of meshes [10, 19, 63-65]. The phenomenon of a fog event and the parameters to obtain the maximum fog water collection efficiency have been described extensively.

From the last 50 years, the altitude range (530 m to 948 m) was tested for the different fog collected in Chile [66]. It is an easy and sustainable technology that collects pure water in some areas of the world. There it counted the variation in the results for the same geographic location and atmospheric conditions. The fog collector consisting of double-layer mesh with a surface solidity ($s = 30\%$) was reported best and recommended for future studies [67]. The s is the solid fraction, or solidity, of the layer ($s = d/h$ for our harp design), the probability that a droplet captured by a layer has a radius in the specific interval (see figure 6C and equation 2).

Since the fog catching technology was invented by Carlos Espinosa in Chile [68], fog catchers started to depend on the designs of the structure to get maximum efficiency, and a large fog collector (LFC) considered the most frequent model utilized in the last decades [68-70]. Polyethylene (PE) and Polypropylene (PP) are the most common meshes being used with fog collectors having 35% s . The triangular structure of PP flat fiber has 0.1 mm thickness, 1 mm width, and pore size of about 10 mm with a shelf life of 10 years [71]. These two polymer meshes, however, are not robust enough to resist high-speed wind. Schemenauer and Joe [65] explained that the fiber width is directly related to the fog droplets being collected. It means the five 1-mm wide ribbons produce a higher yield than a 5-mm wide ribbon. Therefore, a double layer mesh is considered better to be used for 70% s of the surface of the collector, depending on the pattern of fibers overlap.

The mesh structure used by the Shanyengana *et al.*, 2003 [72] was compared with other mesh of different s , construction, and materials but did not measure the efficiency only water collection fabricated with the already known local solidity of 35% used in Standard fog collector (SFC) [64]. When it was changed the s , it concluded that the water yield decreased by enhancing the s for a double layer. Although the yield was 77% and 38% with mesh s of 60% and 90%, respectively.

3.3.1. Standard fog collector (SFC)

Different types of fog collectors are designed concerning their shape and size, and also the mesh material which is used. The standard fog collector is primarily used in commercial studies to assess the amount of fog water that can be collecting at a given location. The construction and use of this smooth mesh sheet are described specifically by Schemenauer and Cereceda [64]. The SFC has a $1 \times 1 \text{ m}^2$ surface area with a base of two-meter off the ground is used to install vertically opposite to the foggy wind path as shown in figure 4A. The large fog collector (LFC) has also been broadly used for fog harvesting [9]. The mechanism of LFC is identical to that of the SFC.

3.3.2. Large fog collector (LFC)

As long as the introductory review was made by Carlos Espinosa in Chile, 1957 [68], fog harvesting projects got greater attention for their highly efficient design, flat-screen large fog collector consider top demand collectors utilized within the final decades [64, 70]. The material used for the LFC depends on the cost and availability so cost-effective locally accessible designs were recommended for the projects because the main purpose is to provide fresh water to needy communities, most of which cannot support the implementation and cost of this to a high level. These programs are financed by the NGOs that are responsible to install the set-up along with its maintenance [10]. The primary design on LFC was presented by Schemenauer and Joe (1989) [65, 73] and further detailed information of the wind passing through and across the collector was given by Bresci (2002) [73]. A pictorial illustration of a large fog collector is given in Figure 4B.

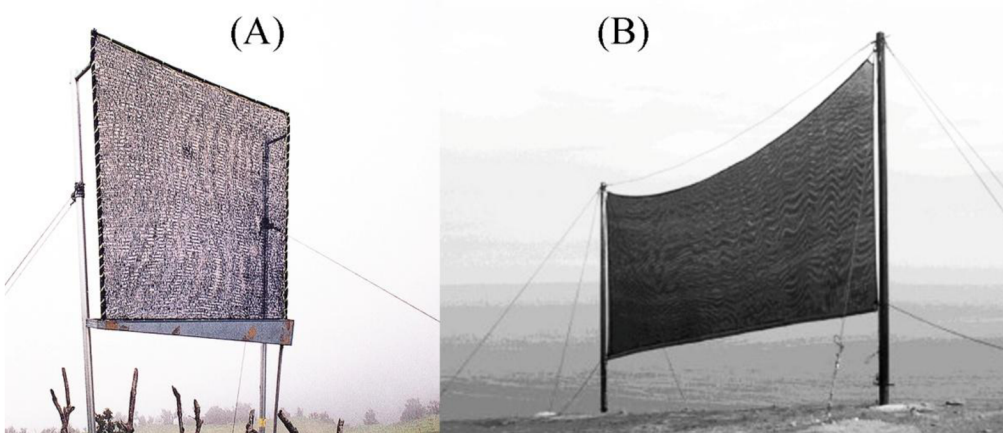


Figure 4: Fog Collectors, (A) SFC (B) (LFC)

Schemenauer and Joe (1989) [65], defined the efficiency of LFC = $\frac{\text{collected water}}{\text{theoretical maximum water}}$.

The characteristics of velocity is complicated to define because of the atmospheric boundary layer [74]. The wind velocity varies with the height and even it is not uniform most of the models measure the LFC efficiency consider the velocity uniform.

3.4. Fundamentals of Fog Collection

The fog called camanchaca (Spanish) mostly has LWC 0.22 to 0.73 gm^{-3} at different positions and occasions. The values noted here are particular for the lower or mid-levels of cloud cumulus [75] and are substantially above what Jiusto, 1981 [76] described for advection or evaporating surface-based fog. The maximum LWC in the camanchaca could be 0.73 gm^{-3} or more depending upon the water availability in the mountains. Higher wind speed reflects the higher values of water collecting efficiency and wind speed inversely proportional to the LWC, so 3.5 m/s wind speed is recommended optimum for the best efficiency by Schemenauer and Joe (1989) [65]. The analysis of wind speed with LWC and fog water collection efficiency is presented simultaneously in Figure 5.

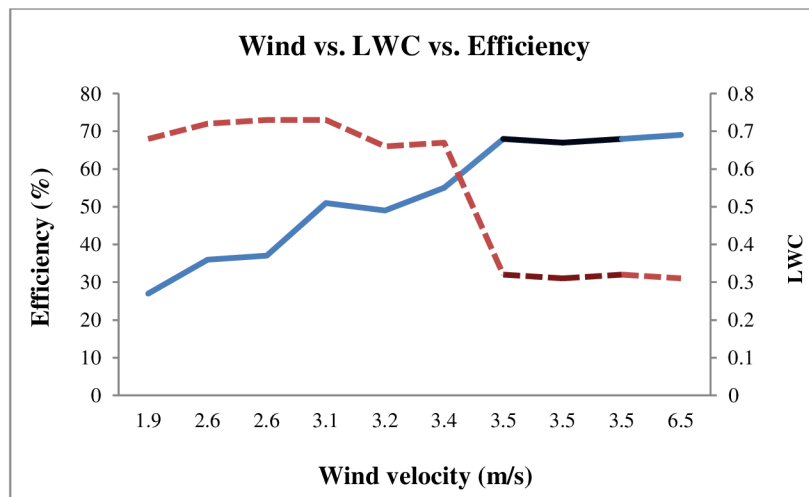


Figure 5: Wind speed is plotted against the efficiency and the LWC. LWC and wind velocity maximize the efficiency of the fog collector

3.5. Multilayer Fog Collectors

To enhance the efficiency of the fog collector, it was proposed to modify the design and fog collector element (FCE). FCE is the material used as a mesh or obstacle in the passage of a fog

stream. A group of researchers recently used a vertical harp structure consist of vertical wire arrays that could harvest three times more fog as compared to mesh netting [17]. Azeem *et al.*, 2010 presented a design for optimally efficient passive fog collectors by focusing on a geometrical relation by the use of multi-layer collectors whose efficiency is much better than the single-layer collector [40].

3.6. Wettability of Fog Collectors

The standard fog collector is primarily used to investigate the amount of fog water that can be harvested at a specific location [77]. The elimination of suspended droplets within the fog stream is a challenge being faced in this mechanism. The typical size of fog water droplets is 5–50 μm float in saturated air [78]. However, coalesces of fog drops may increase the size of droplets ($> 0.2 \text{ mm}$) due to wind and convert to drizzle or rainfall [79]. An ideal fog collector would have to recover most of the liquid fraction from the fog stream and evacuates it to storage quickly. Meanwhile, the gas phase in the stream should pass freely from the collector elements [31]. However, porous collectors have been extensively used in the field of fog harvesting so far [10]. Past research only focused on unmethodical comparisons of collector designs made of synthetic textiles under field or laboratory conditions [11, 69]. Cost-effectiveness and commercial accessibility was the basic reason to not take account the optimization of efficient fog collector, apart from some exceptions [11, 19].

The term wettability is generally used to explain surface modification. The intermolecular interactions between the liquid and solid surface define the nature of surface wettability. Water lover surface called wettable surface or hydrophilic and water repellent surface termed as non-wettable surface or hydrophobic. Surface modifications alter the intermolecular interactions of boundary layers of solids with liquid accomplished variable degrees of hydrophilicity or hydrophobicity [80, 81]. Surface modification influences the fog harvesting performance because wettability adds the pinning strength to the collector element. Similarly, the structural design and geometry of collector elements influence the efficiency of fog collectors [11]. Herein, the main purpose of wettability is to enhance the efficiency of the fog collector and to avoid clogging along with the minimum pinning force.

Indeed, an additional complication is the clogging of the collector by the liquid that has been intercepted. The droplets fill the pores within the collector and thus increase greatly the pressure drop necessary to maintain the flow of gas in the system. Moreover, fog collectors with high droplet capture efficiency have a high rate of water accumulation and also have a high rate of water evacuation to remain efficient. Some investigators have sought to alleviate the problem of clogging by making structural changes to the mesh such as using harp designs instead of crisscrossing thread patterns [17, 82]; because vertical threads have the advantage of letting droplets slide easily under the action of gravity, thus reducing greatly the amount of water present at any time on the mesh. Nature has explored many bioinspired fibers, as observed in the cactus spine, spider webs, Namibian beetle, and *Tillandsia landbeckii*, a plant on the coast of the Atacama Desert of Chile that almost fulfill their water needs from fog [29, 83-85].

Polyethylene (PE) is commonly used for medical and industrial applications on account of its outstanding material characteristics (high chemical resistance, ductility, quick-drying ability, low hardness, and biodegradability) [86]. Aside from the wetting behavior, it has overcome the textile industry, as fast-growing day by day due to simple care properties. The moisture regain (MR) of PE is almost zero and hence moisture does not influence its mechanical properties.

There are two methods to achieve the hydrophobic surface of textile fibers. The first method is based on a hydrophobic self-cleaning phenomenon where water droplets work as an absolute circle and roll out pollutants and dust particles that are stuck on the surface of textile fibers. In this method, the extent of hydrophobicity is determined by the measurement of contact angle. The higher the contact angle, the greater would be the hydrophobic level. Generally, the water contact angle between 120° to 145° is considered as hydrophobic as and lower than 90° is used for hydrophilic surfaces. In the second method, a layer of inorganic materials is applied that works as a hydrophobic surface and protects the textile fiber from wetting. Different types of silanes, silica quartz, and silicon dioxide are some of the examples of inorganic hydrophobic materials. Silane has been used vastly to change the interface of boundary layers of collector elements to fog droplets with hydrophobicity. Most common experimented organosilanes have

one organic substituent and three hydrolyzable substituents. In general, surface modification, the alkoxy groups of the trialkoxysilanes are hydrolyzed to make silanol-containing species [87].

Plasma technology gained interest because of its improved wettability, adhesion, and environmental sustainability especially atmospheric pressure plasma [88]. DBD non-thermal plasma is one of the highly promising technologies reported over the last decade for surface modification due to its improved capacity of enhancing wettability with low power consumption. It is well known that plasma treatments only affect the first few subsurface atomic layers without modifying the overall bulk properties [89].

Recently, it has been reported that surface wettability readily increases the moisture harvesting entertainment, depending on the condition, some outcome has been reported, and it is not clear what type of surface wettability would be perfect for the efficient water collection [40, 90]. Kim *et al.*, 2019 reported a novel fog harvesting method based on ZnO and silver hierarchical micropatterning nanostructures. Their results for the fog collection rate were significant as compared to superhydrophilic and super-hydrophobic surfaces [91]. There are plenty of other researchers who developed biomimetic surfaces for the fog water harvesting process. In another study, Liu *et al.*, 2019 reported super-hydrophilic and superhydrophobic hierarchical nanocrystal patterns on a biopolymer (soy protein). They achieved a maximum water harvesting efficiency of $103 \text{ ml min}^{-1} \text{ m}^{-2}$ that has proposed that the fog harvesting process has the potential to collect water from the moist atmosphere [92]. Gurera and Bhushan, 2020 worked on efficient water collection efficiency through fog harvesting and condensation and designed triangular patterns and conical surfaces that create pressure gradient and accelerate water droplet transportation efficiency. They explained the critical role of the surface area during water collection efficiency. Higher surface area results in higher water collection efficiency and vice versa [93]. In another paper, Gurera and Bhushan worked on the optimization of water collection efficiency and the enhancement of water transportation through different mechanisms. They investigated the effects of different parameters i.e., inclination angle, tip angle, grooves, wettability, surface area, and cone length onto conical surfaces. They concluded that gravity and Laplace pressure are the driving forces responsible

for water transportation [94]. In another study, Song and Bhushan worked on fog and condensation processes to increase the efficiency of a water collector that is designed by the triangular pattern on biomimetic surfaces. They have reported that the combined water collection efficiency of fog and other condensation methods is two times higher than the efficiency of the fog harvesting method alone. Wang *et al.*, 2019 used nanomaterials to develop a super-wettable surface that exhibited excellent efficiency in fog water collection. They used titanium dioxide and silicon dioxide for preparing super-hydrophilic and super-hydrophobic coatings, respectively. The results explained that fog harvesting efficiency and condensation properties of these coatings had been significantly enhanced due to the hydrophilic and hydrophobic regions of nanomaterials [95].

Contact angle hysteresis (CAH) is an imperative physical characteristic of dynamic liquid droplets onto a sliding or tilting surface. The droplet clinging on a vertical surface reflects like a raindrop on the window. The droplet is fallen due to gravity, while CAH stabilizes it in the same place. Consequently, the droplet turns into an asymmetric shape. The contact of the droplet to the vertical surface from the top becomes lean, with a low contact angle, whereas the base looks thick, with a maximum stable contact angle. The difference between the minimum and maximum stable angle from top to bottom is called CAH. This work gives ideas for the necessary surface modification and characterization while developing fog harvesters [96].

3.7. Quality of Fog Water

There are numerous perspectives of water chemistry those of which are very important in fog harvesting techniques. The chemical content of the fog droplets in the atmosphere exceptionally matters before it strikes the collector. There are some sites around the world where fog water and rainwater are being collected together. The composition of water collected by fog harvesting contains a higher concentration of solutes as compared to rainwater harvesting. Schemenauer and Cereceda (1992) reported that the high concentration is caused by excessive sulfates based on chlorine as a seawater tracer element. Soil dust also includes the Fe and Al in fog water content. In some cases, the pH values decrease from 6 to 4 which could easily be treated with a simple method. However; the overall quality of fog water is likely to be

used as an alternative supply of water even collected on a large scale [97]. To check the quality of fog water, two collectors were planted at El Tofo, Chile, and Ashinhaib, Dhofar mountains, Oman. They proved that both sources of water fulfill the WHO (world health organization) drinking water standard. Later on, Eckardt and Schemenauer (1998) [35] discovered that ionic contents calculated in fog water in the desert of Namib near Gobabeb also met the WHO standard. An unpublished report (2008) of the fog harvesting project by the Bavarian water ministry in Eritrea has revealed that water from fog collectors that had flowed through a pipeline to storage at the school's site also complied with WHO standards. A satisfied quality of fog water composition was reported from South Africa [98]. Nevertheless, Strater *et al.*, 2010 [99] found excessive metals and ions content at a coastal spot in Chile. The coal plant or power plant and factory's smoke emission on the west coast of South Africa pollute and inject the chemical mixture into the air that causes impurities in fog water. Generally, the content of fog water composition is safe to drink and could be used for irrigation purposes. If there is doubt of any fog water pollution the water must be tested before drinking as for any other form of water stock. Lastly, it is also possible to use the fog water for a longer period as the quality varies during storage in tanks that is afar the scope of this study.

4. Theory

4.1. Total Water Collection Efficiency (η_{tot})

To formalize the performance of fog collectors, we define, as others have done before [19, 31, 65], the water collection efficiency (η_{tot}) as the water flux coming out of the collector's gutter (J , $\text{g} \cdot \text{s}^{-1} \cdot \text{m}^{-2}$) divided by the liquid water flux of the unperturbed fog upstream of the collector:

$$\eta_{tot} = \frac{J}{LWC \cdot u_{\infty}} \quad (1)$$

Where LWC is the liquid water content of fog and u_{∞} is the velocity of the unperturbed fog flow, which we assume to be orthogonal to the surface of the collector. A typical value of the LWC is $0.2 - 0.5 \text{ g} \cdot \text{m}^{-3}$ while the characteristic fog velocity is $2 - 5 \text{ m} \cdot \text{s}^{-1}$ [65, 100].

It is convenient to define η_{tot} in geometrical terms first by considering how a fog droplet upstream of the collector can ultimately be found in the flux of water " J " coming out of the collector's gutter. The first two stages of collection operate at different length scales (Figures 6B, C). First, we consider what happens at the scale of the entire fog collector (Figure 6C), where the characteristic Reynolds number based on collector size ($l \sim 1-10 \text{ m}$) and unperturbed air velocity ($u_{\infty} \sim 5 \text{ m} \cdot \text{s}^{-1}$) is

$$Re = \frac{u_{\infty} l}{\nu} \sim 10^6$$

Where ν is the kinematic viscosity of air. Incoming fog droplets are part of an airstream which must filter through the collector if the droplets are to be captured. Because the collector is an obstacle to the free flow of the airstream, a fraction of the incoming fog will simply bypass the collector (Figure 6A). The filtered fraction (φ) can be quantified geometrically as the ratio of two areas:

$$\varphi = \frac{A_{\infty}}{A},$$

Where A_∞ is the area for the unperturbed incoming fog flow that will filter through the collector of frontal area A . In the specific case of a square collector (Figure 6A, B), the filtered fraction is

$$\varphi = \left(\frac{l_\infty}{l}\right)^2$$

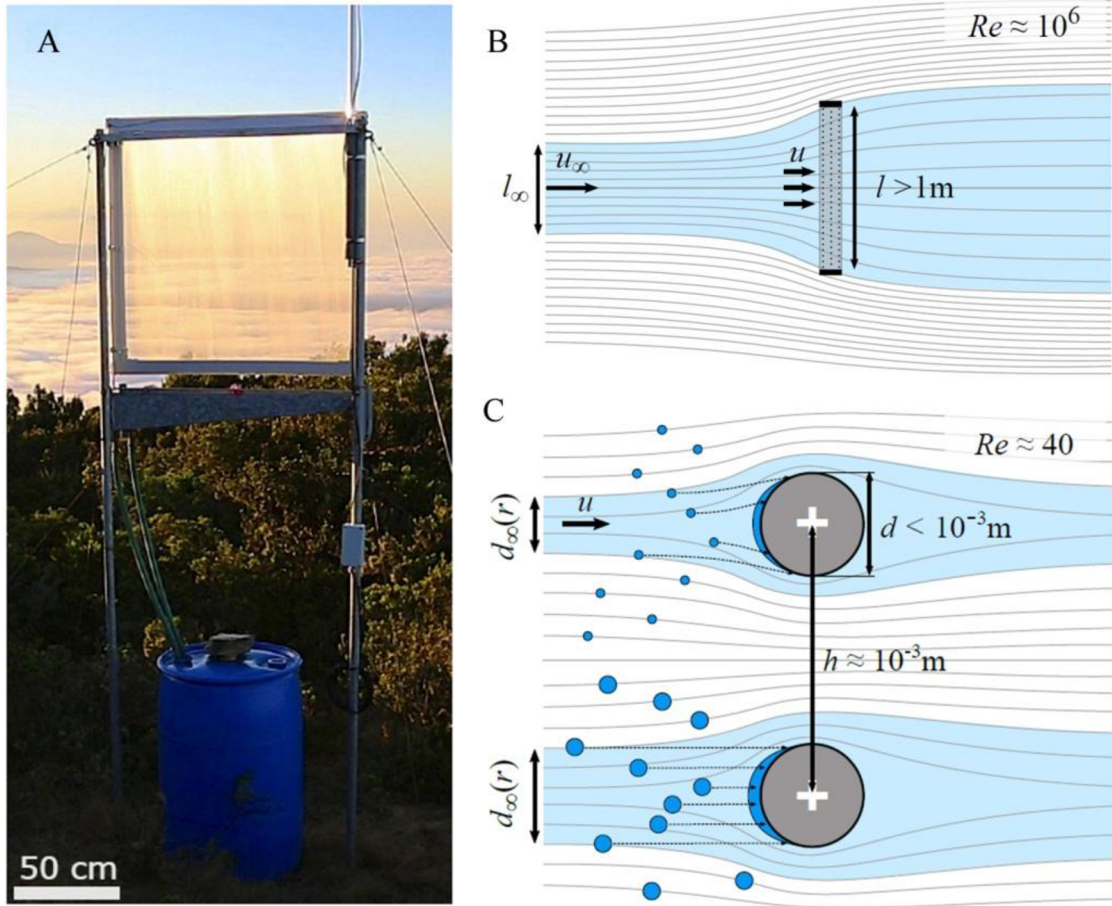


Figure 6: (A) Prototype of a 1 m × 1 m multiharp fog collector with a mesh solidity $s = 0.3$ per

layer and $N = 4$ layers. (B) Top view of the air flow around a fog collector. The typical collector length is $1\text{ m} \leq l \leq 10\text{ m}$. Streamlines are drawn based on wind tunnel experiments by Ito and Garry [101], with square mesh gauze of solidity 0.63 at $Re \approx 10^6$ based on the collector size. (C) Close-up of the air flow around the section of two cylindrical threads of the collector.

The diameter of the threads $d \approx 150 - 160 \mu\text{m}$ for the collector is shown in (B) and the experiments discussed below. $d_\infty(r)$ represents the span of streamlines whose droplets will be intercepted by the thread directly downstream. The top and bottom halves of the diagram show

the interception of the small and large droplets, respectively; dashed lines indicate approximate trajectories of intercepted droplets. Streamlines are based on Gordon's simulations [102] at $Re = 20$ based on the thread diameter

The second collection stage takes place at a microscopic scale and pertains to the droplets transiting through the collector. Of these filtered droplets, only a subset will be on a trajectory that ensures collision with one of the collector elements (Figure 6C). For any given layer of the collector, the probability that a droplet collides with a thread is given by $\frac{d_{\infty}(r)}{d} s$, where the ratio $\frac{d_{\infty}(r)}{d}$ represents the efficiency of inertial impaction for a droplet of radius r (Figure 6C) and s is the solid fraction, or solidity, of the layer ($s = d/h$ for our harp design). Conversely, the probability that a droplet captured by a layer has a radius in the interval $[a, b]$ is

$$s \int_a^b \frac{d_{\infty}(r)}{d} f(r) dr \quad (2)$$

where $f(r)$ is the probability density function for droplet sizes.

Given that the mass of water provided by a droplet scales with r^3 , the relative contribution of droplets to the capture efficiency is

$$s \int_a^b \frac{d_{\infty}(r)}{d} m(r) dr, \quad (3)$$

Where

$$\int_a^b m(r) dr \approx \left(\frac{\int_a^b r^3 f(r) dr}{\int_0^{\infty} r^3 f(r) dr} \right) \quad (4)$$

$\int_a^b m(r) dr$ is the mass fraction of liquid water contained in droplets with radius in the interval $[a, b]$ [103].

Finally, to these two processes, we should add the drainage efficiency (η_{drain}) [19, 31]. The drainage efficiency represents the fraction of the intercepted volume of water that ultimately

reaches the tank of the collector. The drainage efficiency may be reduced by re-entrainment of captured droplets under high wind conditions [104] and potential leaks in the gutter and pipe leading to the collector's tank.

In the case of a single-layer collector, the three processes detailed above lead to the following total water collection efficiency:

$$\begin{aligned}\eta_{tot} &= \eta_{AC}\eta_{capt}\eta_{drain} \\ &= \underbrace{\left[\frac{A_{\infty}s}{A}\right]}_{\eta_{AC}} \underbrace{\left[\int_0^{\infty} \frac{d_{\infty}(r)}{d} m(r) dr\right]}_{\eta_{capt}} \eta_{drain}\end{aligned}\quad (5)$$

Where η_{AC} is the Aerodynamic Collection Efficiency (ACE) introduced by Rivera [19]. When considering a collector with N layers, the total collection efficiency takes the form:

$$\eta_{tot} = \frac{A_{\infty}}{A} \left[1 - \underbrace{\int_0^{\infty} \left(1 - \frac{d_{\infty}(r)}{d} s\right)^N m(r) dr}_{\text{lost mass fraction}} \right] \eta_{drain}\quad (6)$$

where the term $\left(1 - \frac{d_{\infty}(r)}{d} s\right)^N$ is the probability that a drop of radius r traverses the N layers of the collector without being intercepted. Consequently, the integral represents the mass fraction of liquid water that filtered through the collector without being intercepted.

Three tacit assumptions were made to arrive at Eq. (6). These assumptions are listed here in order to define clearly the range of validity of our result. First, we assumed that the incoming airflow both far-field and just upstream of the collector is orthogonal to the collector's surface. We justify this assumption because; the optimum fog collectors are quite porous, with approximately ~80% of the incoming fog flow passing through the collector. In this regime, the air velocity has a negligible component tangential to the collector surface, so the interaction of the airflow with the collector filaments does not depend on the position within the collector.

Second, we assume that $\frac{d_\infty(r)}{d}$ is constant at all locations within the collector. This assumption implies a uniform mesh such as the harps under consideration but would have to be modified for meshes made of intersecting weft and warp threads and potentially differing in their size and shape. Third, in deriving the lost mass fraction, we make the hypothesis that the distance between the layers is sufficiently large to allow the fog stream to regain uniformity before reaching the next layer. As we will show below, the optimal interlayer spacing ranges between 6 and 9 mm, which is at least 40 times greater than the characteristic thickness of the layers in our prototypes.

4.2. Maximizing η_{tot}

Because Eqs. (5) and (6) are geometrical definitions of η_{tot} , they are valid irrespective of the fluid mechanics model that might be developed to quantify the collection efficiency. Ideally, we would like to design the collector such that all steps in the collection of fog droplets are maximized to achieve a total water collection efficiency approaching unity. Our goal in this section is to demonstrate that η_{AC} is the only component of η_{tot} that involves some fundamental design tradeoff.

We begin with the drainage efficiency η_{drain} which is included in Eqs. (5) and (6) to take into account the possibility that captured fog droplets are re-entrained by the airstream or otherwise lost due to leaks in the system. Although leaks need to be considered carefully in any implementation of a fog collector, they are outside the scope of a fluid mechanics analysis. Re-entrainment needs to be considered more carefully.

Two ways to eliminate re-entrainment are (*i*) the use of multi-layer collectors to allow re-entrained drops to be re-captured by a layer farther downstream [30] and (*ii*) the reduction in the size of the drops clinging to the collector surface so that the drag on these drops does not exceed the critical value that would cause them to detach. These design requirements are in fact among those put forward to optimize the other aspects of the collection process; therefore the

drainage efficiency will be optimized *de facto*. In what follows, we set $\eta_{drain} = 1$ and focus on the other terms of Eqs. (5) and (6).

At the operational *Re* number of fog collectors, the ratio $\frac{d_\infty(r)}{d}$ reflects a deposition mechanism by inertial impaction [20]. For a droplet of radius r , the efficiency of the impaction mechanism follows the relation [20, 105]:

$$\frac{d_\infty(r)}{d} = \frac{Stk}{Stk + \pi/2} \quad (7)$$

Where $Stk = \frac{2\rho_\omega r^2 u}{9\mu d}$ is the Stokes number, ρ_ω is the density of the liquid, u is the velocity of the air stream, μ is the dynamic viscosity of air, and d is the diameter of the thread. This efficiency increases with increasing Stk ; however, we note from the definition of Stk that the thread diameter " d " is the only parameter that can be tuned in the context of a passive fog collector. Because Stk increases for decreasing d , the width of the elements on which droplets are impacted should be reduced to a minimum. More precisely, Labbé and coworkers [20] demonstrated that the size to be considered is the diameter of the thread with the water film or drops covering it. The reduction in the size of the collecting elements can be done at constant solidity and without compromising other steps of the fog collection process.

Consequently, the geometrical ratio $\frac{d_\infty(r)}{d}$ can be made as close to unity as one desires, although maximizing $\frac{d_\infty(r)}{d}$ for all droplets, size classes are unwarranted since the smallest droplets are the most challenging to capture, and yet they represent a vanishingly small fraction of the total LWC of fog [100].

In what follows, we consider a small operating size for the collecting elements so that $d_\infty \rightarrow d$. In this limit, Eq. (6) becomes:

$$\lim_{d_\infty \rightarrow d} \eta_{tot} = \eta_{AC} = \underbrace{\left[\frac{A_\infty}{A} \right]}_{\varphi} \underbrace{[(1 - (1 - s)^N)]}_{\chi} \quad (8)$$

This equation captures in its most general form the Aerodynamic Collection Efficiency (η_{AC}); that is, the fraction of droplets in an unperturbed upstream flow of area A that are both filtered by (ϕ), and incident to (χ), the elements of a multi-layer collector.

The ACE is of special significance because it encapsulates the fundamental trade-off in the design of efficient fog collectors. While the incident fraction χ increases with increasing solidity s and the increasing number of layers N , the same parameter changes reduce the collector porosity and therefore decrease the filtered fraction ϕ .

4.3. Fluid Mechanics Prediction of A_∞ / A

Determining ACE for a specific collector involves finding the ratio $\phi = \frac{A_\infty}{A}$ using the design parameters of the collector, such as the solid fraction of the individual mesh layers and the total number of layers. We first note that incompressibility of the flow together with mass conservation imply $Au = A_\infty u_\infty$ (Figure 6B). Therefore, the geometrical definition of the filtered fraction is also a statement about the ratio between the mean velocity across the collector mesh and the velocity far upstream of the collector, that is:

$$\phi = \frac{A_\infty}{A} = \frac{u}{u_\infty} \quad (9)$$

We follow the many earlier studies of fluid flow through and around porous structures that equate to two alternative definitions of the pressure drop across the porous material, the first one at the scale of the porous medium and the second one at the scale of the far-field flow. At the microscopic scale, the pressure drop is

$$\Delta P = k \frac{\rho_{air} u^2}{2} \quad (10)$$

where ρ_{air} is the density of air and k is the pressure drop coefficient for the flow of an inviscid fluid through a porous medium. This equation arises naturally from Bernouilli's principle

[103]. As we shall see, since " k " is typically not constant over a very large range of velocities, the pressure drop coefficient is necessarily expressed in terms of the solid fraction of the medium and the Reynolds number. At the scale of the entire collector, the pressure drop across the mesh is also related to the drag coefficient C_D ,

$$\Delta P = \frac{F_D}{A} = C_D \frac{1}{2} \rho_{air} u_{\infty}^2 \quad (11)$$

because the drag force F_D per unit area on the screen must equal the pressure drop. Eq. 11 represents the so-called "form drag" and is valid for blunt objects at high Reynolds numbers, which is the case for fog collectors [106]. Equating the two pressure drops we obtain the filtered fraction

$$\varphi = \frac{A_{\infty}}{A} = \frac{u}{u_{\infty}} = \sqrt{\frac{C_D}{k}} \quad (12)$$

This equation has been used in its various forms by Taylor [107], Koo and James [108], Steiros and Hultmark [109] among many others.

There is no consensus on how to express the drag coefficient C_D and the pressure drop coefficient (k) in terms of the design parameters of the collector mesh. To our knowledge, the most recent and most complete treatment is due to Steiros and Hultmark [109] (later termed Steiros 2018); who extended the earlier work of Koo and James [108] by including the so-called "base-suction" and thus obtained accurate predictions of the drag coefficient over the entire range of solid fractions. According to their model, the drag and pressure drop coefficients are

$$C_D = \frac{4}{3} \frac{(1-\varphi)(2+\varphi)}{(2-\varphi)} \quad (13)$$

$$k = \left(\frac{1}{(1-s)^2} - 1 \right) - \frac{4}{3} \frac{(1-\varphi)^3}{\varphi^2(2-\varphi)^2} \quad (14)$$

Substitution of these two relations in Eq. 12 gives an implicit relation for the filtered fraction as a function of the solidity. Finally, since k is the coefficient for the pressure drop across one layer of the collector, a conservative estimate for the total pressure drop across multiple layers is obtained by multiplying k by the number of layers in the collector. The additivity of the pressure drop coefficient was confirmed by Eckert and Pflüger [110] when the distance between the screens is sufficiently large. Idel’Cik estimates that the pressure drop across multiple layers is additive as long as the distance of separation between the layers exceeds 15 times the size of the threads (Idel’Cik, [111] page 291).

4.4. Models for Filtered Fraction

We consider below three alternative models for predicting the filtered fraction φ for a fog collector constituted of N layers, each with shade coefficient s . As stated in the main text, the approach taken by most models is based on the following relation for the filtered fraction:

$$\varphi = \frac{A_\infty}{A} = \frac{u}{u_\infty} = \sqrt{\frac{C_D}{k}} \quad (12)$$

Therefore, we seek to express the drag coefficient C_D and pressure loss coefficient k in terms of N and s .

4.4.1. Glauert 1932 Model

Glauert and coworkers [112] presented one of the first detailed analyses of the flow through and around a porous structure. Treating the flow in the porous medium as a series of sources, they arrived at the following relations:

$$C_D = \frac{k}{\left(1 + \frac{1}{4}k\right)^2}$$

and

$$k = s \left(\frac{1}{(1-s)^2} - \frac{2}{3} \right)$$

Although the equation for C_D never appears in this form in their paper. The first relation was re-affirmed by Taylor [113] using two different approaches. However, as was clear at the time, the relation does not admit drag coefficients greater than 1 even in the limit of k approaching infinity (a solid plate) while it is known that the drag coefficient for a square plate is in fact 1.18 in the range of Re numbers of interest. Luckily, the equation is most robust for small k (small shade coefficient), which is the regime of interest for fog collectors. Taylor [107] states that the equation could be valid for $k \leq 4$.

4.4.2. Rivera 2011 Model

Rivera [19] took a slightly different approach by considering the flow through and around the collectors as the superposition of two distinct flow fields with the condition $u_\infty = u + \hat{u}$, where u_∞ is the velocity of the unperturbed upstream flow, u is the velocity of the uniform flow that filters through the porous collector and \hat{u} is the velocity of the flow associated with a solid collector. Rivera then equates the pressure drop for the two components of the flow field based on Bernoulli's principle:

$$\Delta p = \frac{\rho \hat{u}^2}{2} \hat{C}_D = \frac{\rho u^2}{2} k$$

And since $u_\infty = u + \hat{u}$, we have,

$$\frac{\rho (u_\infty - u)^2}{2} \hat{C}_D = \frac{\rho u^2}{2} k$$

rearranging gives,

$$\left(\frac{k}{\hat{C}_D} \right)^{1/2} = \frac{u_\infty - u}{u}$$

and finally,

$$\varphi = \frac{1}{1 + (k/\hat{C}_D)^{1/2}}$$

where $\hat{C}_D = 1.18$ is the drag coefficient corresponding to a solid ($s = 1$) collector with a square aspect ratio. For the pressure drop coefficient, the empirical relation given by Idel'Cik [111] was selected:

$$k = 1.3s + \left(\frac{s}{1-s} \right)^2$$

4.4.3. Koo1973 Model

Koo and James [108] revisited the model of Taylor [107] by considering the flow through a porous medium as equivalent to distributed sources. The problem was solved to ensure the conservation of mass and momentum across the mesh, leading to the implicit relations:

$$k = \frac{2Dk + (Dk)^2}{(1 + Dk)^2} \left(1 + \frac{Dk}{2}\right)^2$$
$$C_D = \frac{k}{\left(1 + \frac{1}{2}Dk\right)^2}$$

where D is the source strength. Because Koo and James [38] were mostly concerned about the relation between k and C_D , they did not try to express k in terms of the shade coefficient. We can however use Idel’Cik’s [111] empirical relation $k = 1.3s + \left(\frac{s}{1-s}\right)^2$ to close the problem.

5. Research Methodology

This research part includes the materials and methodology for the development of an efficient fog collector. The optimal design of multilayer fog collector and the effect of wettability have been discussed experimentally and theoretically.

5.1. Materials

Cotton spun yarn, polyester, polypropylene, and polyethylene were used to initiate the experiments for the best possible selection. Cotton ring spun yarn was collected from the KMI lab, TUL while all the polymers were obtained from the Hahl Filaments GmbH, Munderkingen, Germany.

Table 1: Specification of all the materials used for the study

Material	Color	Diameter (mm)	Density (g/cm ³)
Cotton Spun Yarn	Black	0.16	1.54
PES monofilament		0.15	1.39
PE monofilament	Transparent	0.15	0.95
PP monofilament		0.15	0.92

Various systems are being used to measure the yarn fineness in the textile industry but here we mentioned the diameter in millimeters (mm) for our results. Laboratory microscope was used to measure the diameter. PE monofilament was used to exercise the experiential part due to its favorable properties e.g. weather resistance, low water absorbency, recyclable, biodegradable, cheap, and easily available [46].

5.2. Collector Design

Raschel Mesh was obtained from the bioengineering laboratory, Universidad Adolfo Ibáñez-Campus Viña del Mar, Chile. The design of the mesh is much porous so double layer is used for fog collection. The ribbon-like structure and high porosity of the mesh was considered the major drawback to collect a high yield of fog water as shown in figure 7 (A, B).

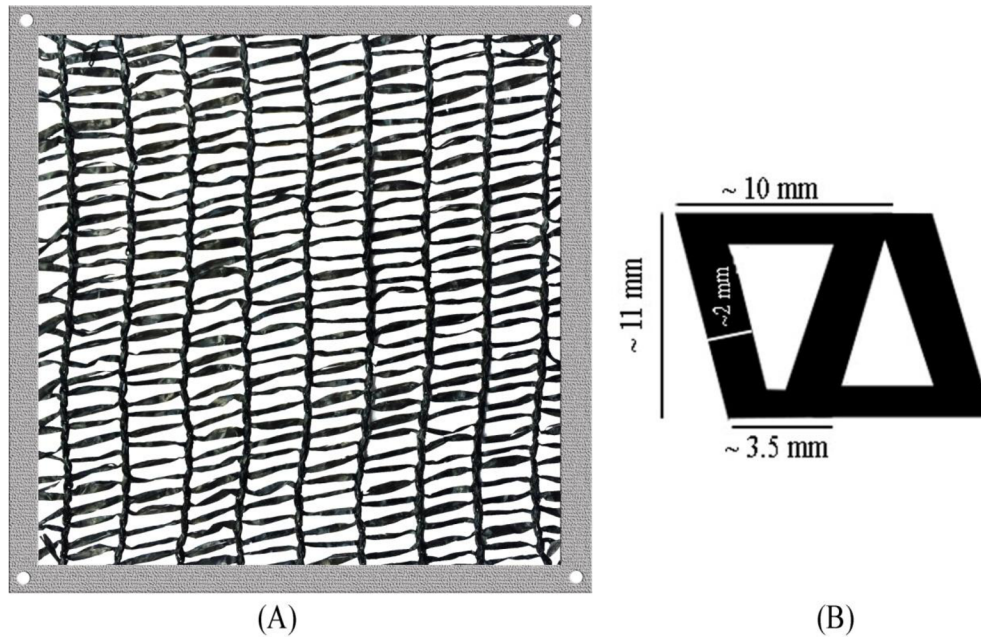


Figure 7: Knitting pattern Raschel mesh. (A) Prototype 100 mm×100 mm. (B) Structure of mesh

5.2.1. Construction of prototypes

Multi-layered collectors were built using fast prototyping tools. Square plexiglass frames with a 100 mm × 100 mm central open area were cut using a laser cutter (Ready Cut) as used in Figures 7A and 8A. Evenly spaced notches (typical spacing: $1 \text{ mm} \leq h \leq 2 \text{ mm}$) were made in the upper and lower edges of the frame to hold polyethylene monofilaments ($d = 150\text{-}160 \text{ }\mu\text{m}$) into a vertical harp arrangement (see figure 9).

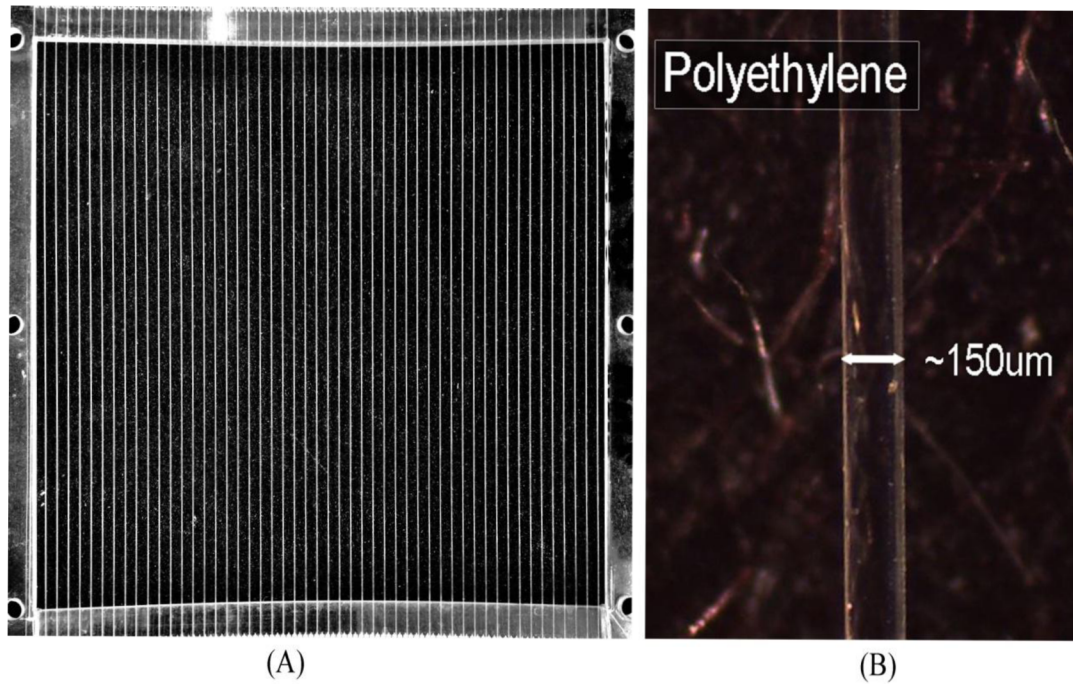


Figure 8: Harp collector built with PE monofilament. (A) Prototype 100 mm \times 100 mm. (B) microscopic view of PE monofilament

These frames were then stacked with different inter-layer spacing to form a multilayer fog collector. The experiments reported here were done with a staggered relative alignment between successive layers. All the trials with staggered and in-line arrangements of layers were measured to fix it for the rest of the experiments. Note, however, that the staggered or in-line arrangements of layers had no significant effect on the performance of the collector. Figure 16 illustrated in the results confirm the verdict.

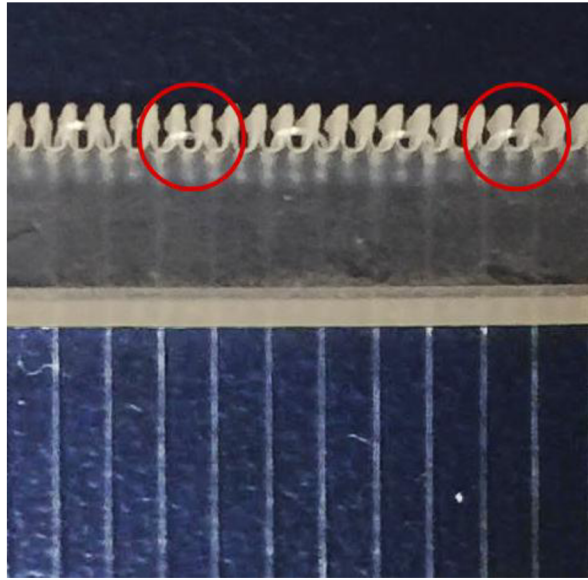


Figure 9: Construction of harp collector with evenly spaced notches

5.3. Measurement of Aerodynamic Collection Efficiency

Flow experiments were performed with an open-jet wind tunnel developed specifically to measure the efficiency of fog collector prototypes under natural conditions. The tunnel consists of two elements: a lower nebulization chamber for fog production and an upper flow chamber to accelerate the fog cloud and guide it into a uniform jet (Figure 10). The nebulization chamber contained ≈ 50 L of water within which was immersed a 300 W 12-head ultrasonic nebulizer (Model DK12-36). The fog produced in this chamber was injected into the upper chamber by a 16 W, 200 mm \times 200 mm ventilation fan. Within the flow chamber, an array of 16, 80 mm \times 80 mm, computer fans accelerated the fog toward a contraction that converged the fog stream to a jet of 140 mm \times 140 mm in cross-section. Both the ventilation fan and the array of computer fans were powered through variable voltage transformers allowing us to set the jet velocity in the range 0.1 – 4.2 m s⁻¹. A honeycomb filter was placed at the upstream end of the contraction to eliminate turbulence and provide a homogeneous fog flow.

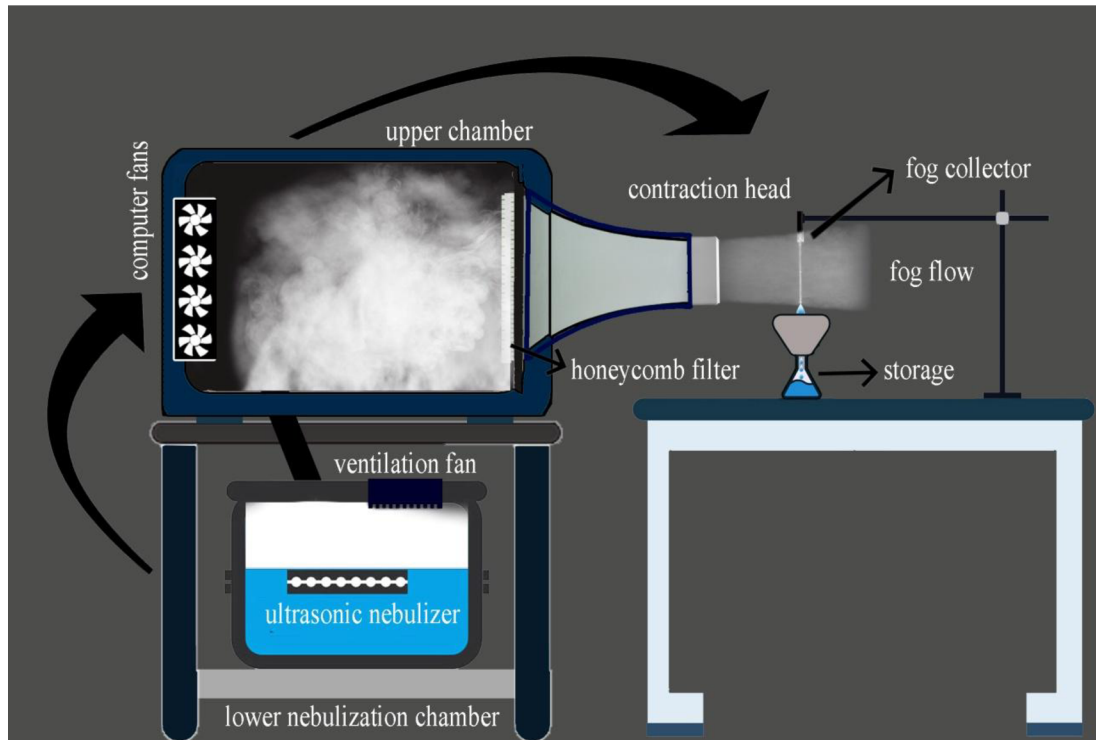


Figure 10: Flow diagram of the platforms to quantify the two stages of fog droplet collection

The flow of fog through and around the collector prototypes was visualized by using a Phantom V611 high-speed camera equipped with a Canon EF 100–400 mm telephoto zoom. Images were acquired at a rate of 4000 fps (exp 240 μ s) with a camera resolution of 1024 \times 768 pixels and an image scale of 270 μ m/pixel. Analysis of the flow pattern was performed using a Matlab program first developed by Dr. A. F. Forughi at the University of British Columbia (Vancouver, Canada) and made freely available on Github (<https://github.com/forughi/PIV>).

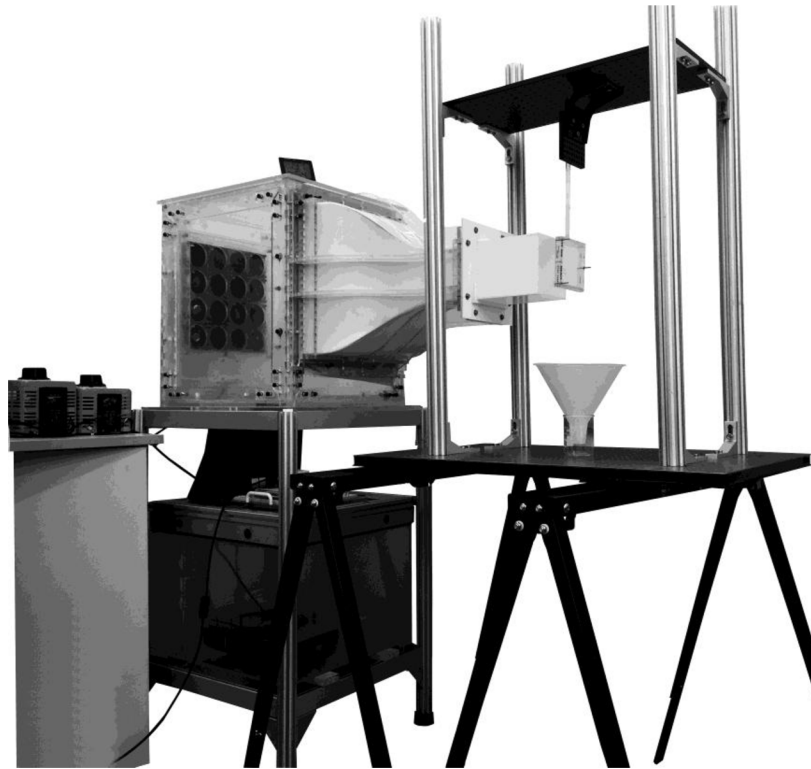


Figure 11: Wind tunnel platform used to measure the large scale flow field

5.3.1 Yield measurements

To measure the yield, the prototypes were hung at a distance of 100 mm from the opening of a wind tunnel equipped with a fog chamber (see Figures 11 and 12A). The higher distance between the opening of a tunnel and prototype results in stray of fog fraction while lower distance could generate pressure inside the wind tunnel. The water collection rate was found slightly higher when the distance between the opening of a wind tunnel and prototype was 100 mm as shown in figure 12B. The water was collected in a funnel leading to a graduated cylinder. Collection occurred over a total time interval of 15 minutes following an initial saturation period of 5 minutes.

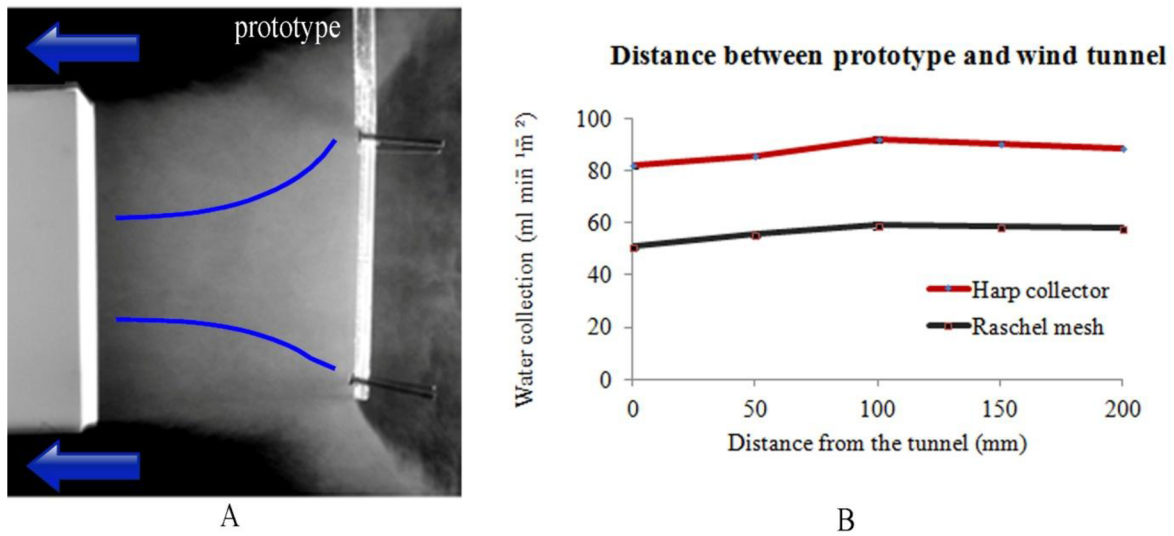


Figure 12: Measurement of the yield. (A) The prototypes from the opening of a wind tunnel. (B) Optimized the distance between wind tunnel and prototype

5.4. Wettability

The chemical structure of PE consists of straight carbon-hydrogen chains, thus permitting diverse surface modifications. The PE monofilaments of diameter 150 μm were acquired from HAHN Filaments Company, Germany. Some samples were processed for hydrophilicity and exposed to dielectric barrier discharge (DBD) plasma. Some samples were experimented with for hydrophobicity and exposed to silane treatment. For a better comprehension of the methods linked with adhesion at the interface, a systematic study of surface properties, both physical and chemical is very important. Herein, the main purpose of wettability is to enhance the efficiency of the fog collector and avoid clogging along with the minimum pinning force. Moreover, fog collectors with high droplet capture efficiency have a high rate of water accumulation and retention. Such fog collectors are not favorable for fog water harvesting.

5.4.1. Plasma treatment with DBD reactor

Plasma treatments were performed on PE monofilament with a parallel-plate DBD-system at medium pressure. The reactor consists of two copper electrodes (upper and lower electrodes)

covered with glass plates. A monofilament sample was placed onto the lower electrode to achieve a reproducible discharge gas composition for 5 minutes. For DBD plasma discharges three different samples were prepared with dry air treatments. A vast range of literature reviews has been reported that the plasma-treated polyethylene fibers with different gasses are used to enhance the energy absorption and interfacial shear strength [114, 115].

5.4.2. Silane treatment

In our experiments, silanization of monofilament PE was performed with dichlorodimethylsilane. For this purpose, silane 10 g/l was applied to the fabric under the pad-dry-cure method. 3 dips were performed and the time of each dip was 1 min. The drying temperature was 70 °C and the curing process was done to fix the silane. After that, hydrophobic performance was evaluated by contact angle measurement.

5.4.3. Characterization

Surface topography was characterized by XE-70 Atomic Force Microscope (AFM) system (Park Systems™, Suwon, South Korea). The static contact angle was measured by using Krüss Easy Drop optical system (Hamburg, Germany). A 0.5 microliter water droplet was used to compute the contact angles automatically within 3s using the Laplace-Young curve-fitting procedure. The dynamic contact angle was performed by growing the volume of the droplet on the FCE from 0.5 μl to 1 μl . CAH was measured from the advancing and receding contact angles. All of these calculations were taken at room temperature. Computer software ImageJ was used to measure the CAH.

5.4.4. Fog generator

To measure the yield of fog water collection, the samples of treated and untreated monofilaments were hung with vertical stand at room temperature and 100% humidity as illustrated in Figure 13. The TWIN-humidifier (Brno, Czechia) was utilized to generate fog

with a velocity of 4-4.5 m/s. The aerosol particle size or mass median diameter (MMD) was approximately 5 micrometers. The hanging specimens were exposed to a fog stream for 30 minutes and then measured the yield of collected fog droplets.

Table 2: Properties of TWIN-humidifier

Model	Voltage (V)	Frequency (Hz)	Watt (W)	Flow rate (mm/mint.)	Particle size (μm)
SPS-702	220-240	50	30	0.4	5



Figure 13: The diagram of the experimental setup for fog collection

6. Results and Discussion

The study consists of two major parts; the first is about the optimal design of multilayer fog collectors and the second part is about the surface wettability of vertical harps for fog collection. The first part was started with four different materials (threads) to construct the fog collector. Cotton yarn was compared with other filaments (PES, PP, and PE) and found that spun yarn is not suitable for the study due to water retention in the structure as shown in figure 14. Polyethylene monofilament was selected for the rest of the study due to its versatile properties and highly reported in the previous study.

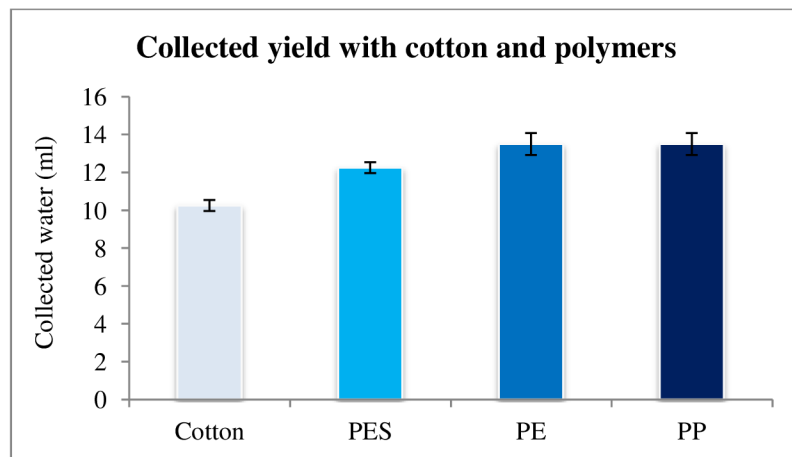


Figure 14: Yield collected of four different collector elements after 15 minutes with one layer

6.1. Optimal Design of Multilayer Fog Collectors

We designed a wind tunnel and optimized some of the variables to execute the experiments. We optimized the distance between two adjacent fog collector elements and the distance between wind tunnel and prototype as shown in figure 9 and figure 12.

For the control parameters, we also fixed the multilayer arrangement in the prototype. Figure 15A illustrated that the stagger and in-line arrangements of the harp are not affecting the total yield collection when using multilayer. Figures 15B and C visualized the in-line and stagger arrangements of layers in a multilayer fog collector.

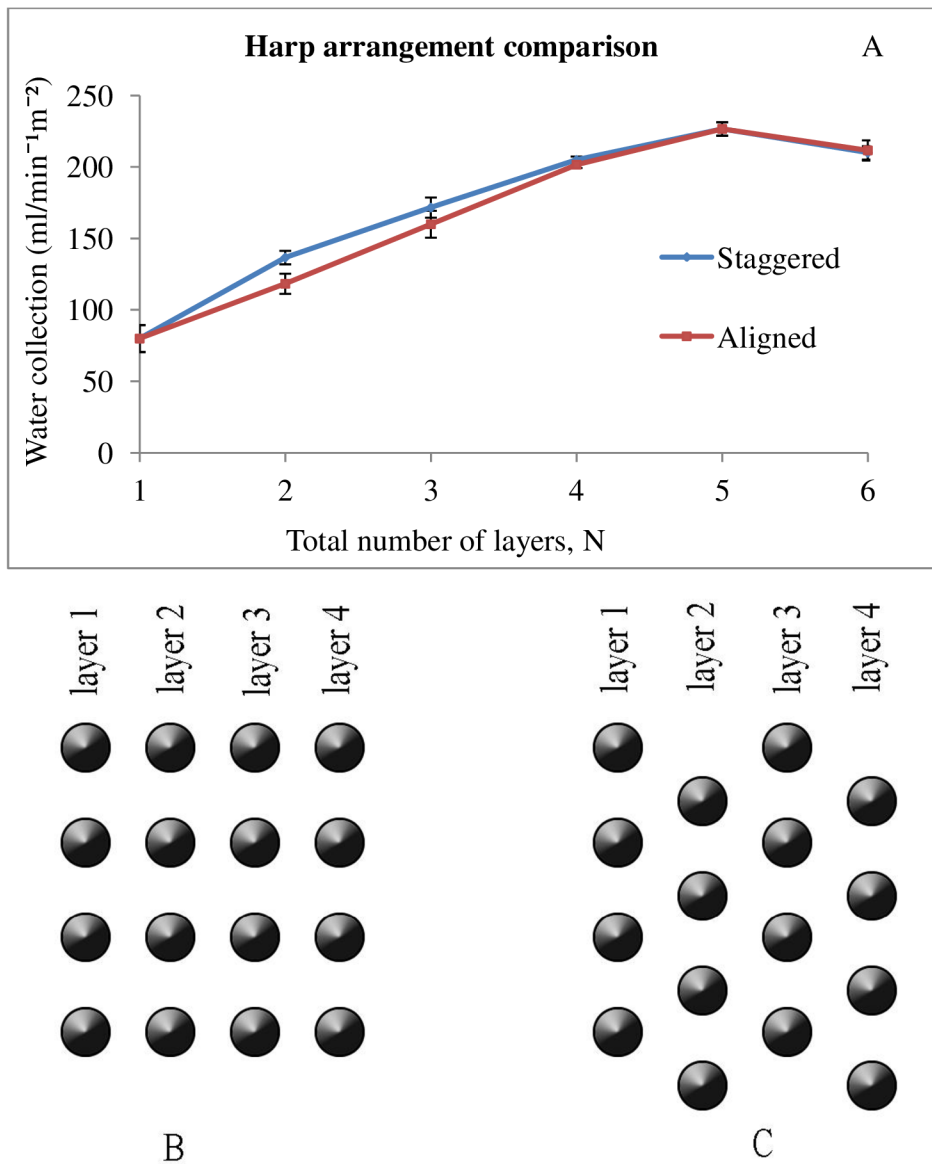


Figure 15: (A) Multilayer arrangement comparison. (B) In-line arrangements of layers. (C) Stagger arrangements of layers

To optimize the distance between the two layers of fog collection it was set a series of experiments by varying the distance. Fourteen sets of experiments were performed by adjusting the space 0-36 mm between the adjacent layers. The interlayer spacing of 6 mm was found best to get maximum yield and allow the fog flow to be homogenous for striking the next layer as shown in figure 16.

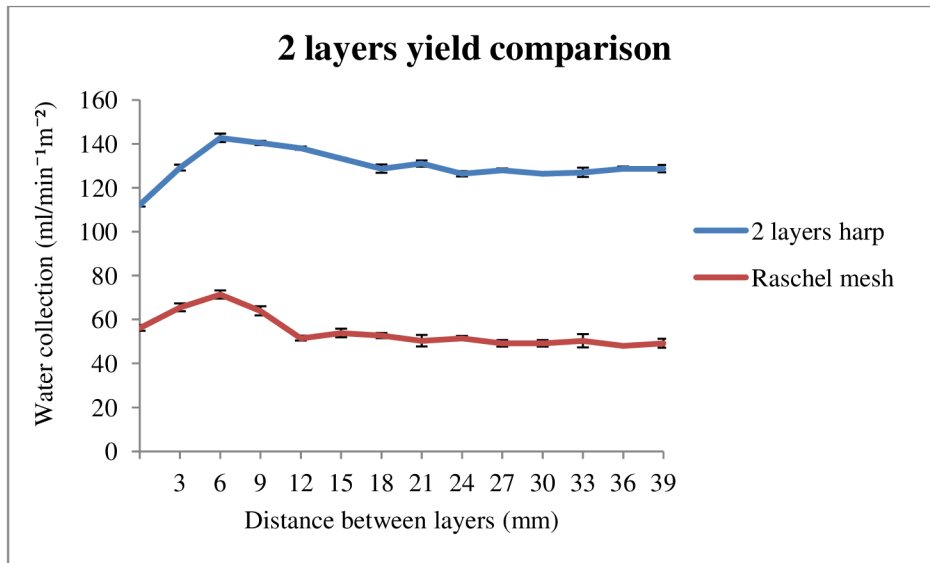


Figure 16: Effect of interlayer spacing on the yield of multilayer collectors

6.1.1. Efficiency of multilayer fog collector

To maximize the overall collection efficiency, we must seek a high filtered fraction (ϕ) and a high incident fraction (χ). However, these quantities are maximized at opposite ranges of the parameters s and N (Figures 17A, B); this fact constitutes the central trade-off of fog collection. The results obtained in the previous section allow us to calculate the maximum ACE found at some intermediate values of these parameters.

As can be noted in Figure 17B, the incident fraction depends very nonlinearly on N which, at a single glance, establishes the notable advantage offered by multilayer designs. In a single-layer

collector, the incident fraction cannot be maximized to unity, as this would imply complete obstruction of the mesh and thus no airflow through the collector.

The use of several layers decouples, at least partially, the fluid mechanical processes behind the filtered fraction and the incident fraction. It is therefore possible to design the collector such that nearly all upstream droplets are on a collision course with one of the collector elements while maintaining the solidity significantly below unity (Figure 17B).

Even for a relatively modest 5-layer collector, a solidity as low as 0.5 can already guarantee a near maximal incident fraction (Figure 17B). The possibility of greatly increasing the incident fraction for intermediate solid fractions is the reason why multilayer collectors can be much more efficient. Moreover, because the equation for the incident fraction is purely geometrical, there is no doubt about the general validity of this conclusion.

Computation of the aerodynamic collection efficiency $\eta_{AC} = \chi\phi$ for a broad parameter range indicates that it reaches a maximum of 49% for $N = 10$ (Figure 18). In contrast, single-layer collectors are confined to the line $N = 1$ and can reach a maximal ACE of only 30% at an operational solidity slightly above 0.5.

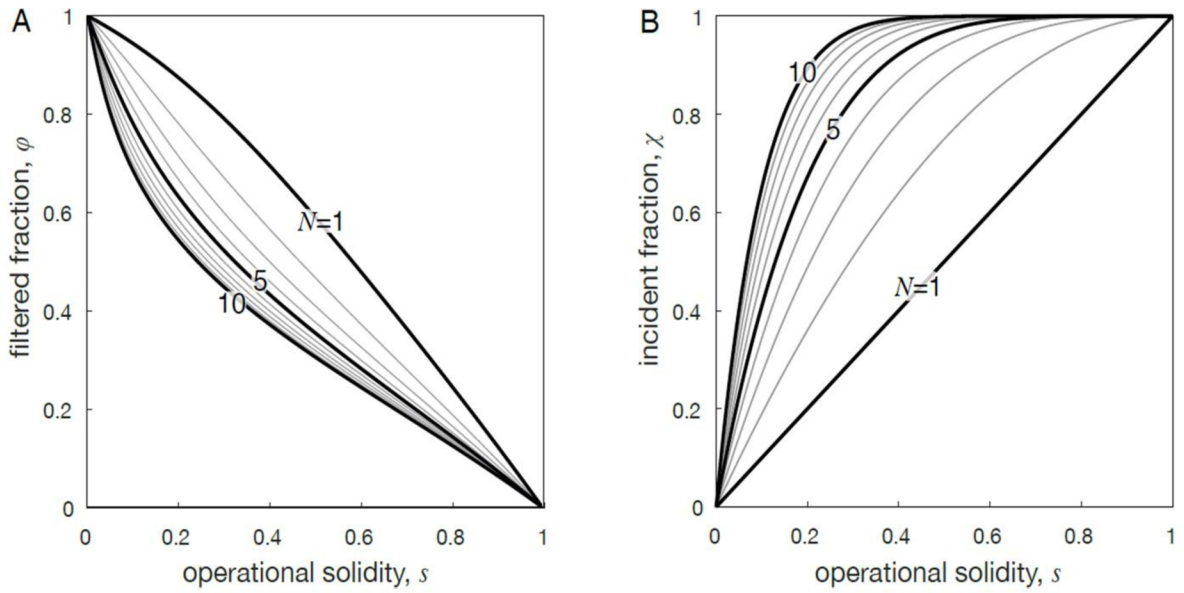


Figure 17: Aerodynamic collection efficiency for multi-layer fog collectors. (A) Filtered fraction predicted from the Steiros2018 model (Eqs. 12-14). (B) The incident fraction computed from geometrical considerations (Eq. 8, second term on the RHS)

Increasing the number of layers beyond 10 increases the ACE further; with the theoretical possibility of reaching an ACE of unity for a very large N (Figure 19). This limiting behavior raises the question of how many layers should be used in practice.

An answer emerges when considering the contribution to the total ACE made by each new layer (Figure 19). Beyond $N = 5$, the relative increase in ACE becomes vanishingly small. Therefore, considerations about the most efficient use of available materials would suggest that the number of layers should be limited to ~ 5 , at least in the limit where $d_\infty \rightarrow d$.

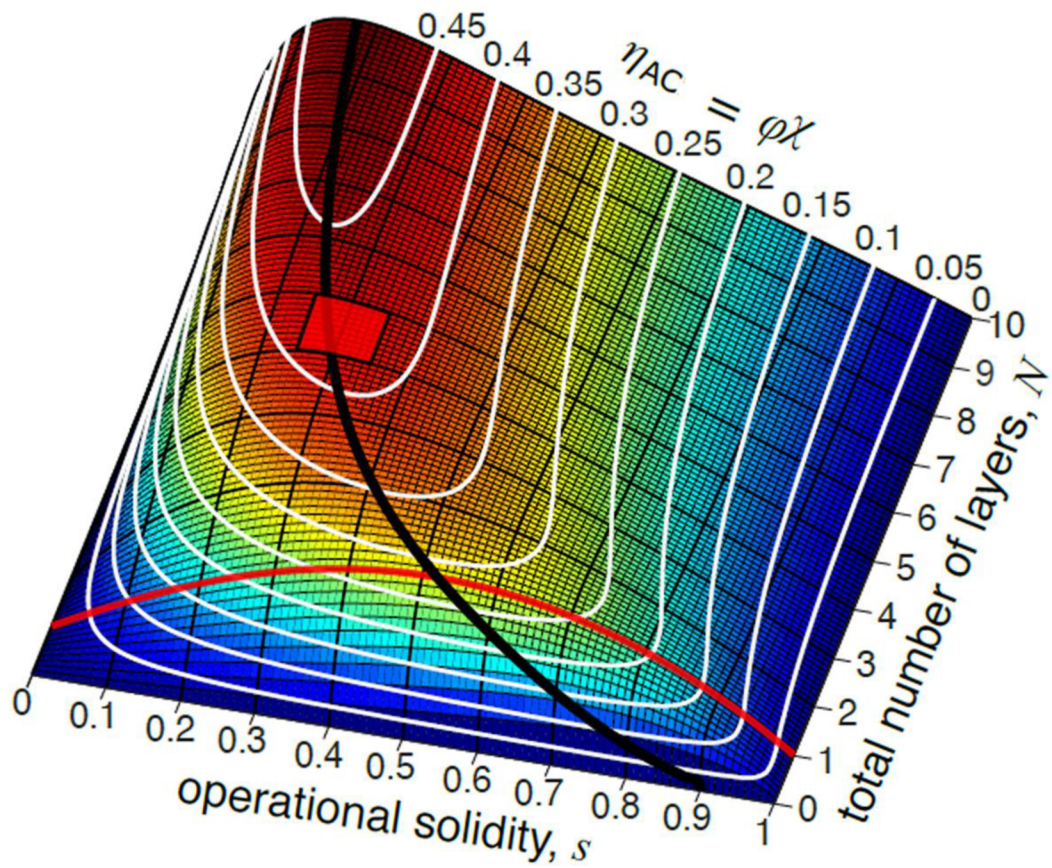


Figure 18: The ACE Ridge - a 3D representation of ACE as a function of the two control parameters s and N . A maximum ACE of 0.49 is observed for 10 layers, each with an operating solidity of 0.17. Single-layer collectors are confined to the line $N = 1$ and have an ACE below 0.3. (Note: we have treated N as a continuous variable for illustration)

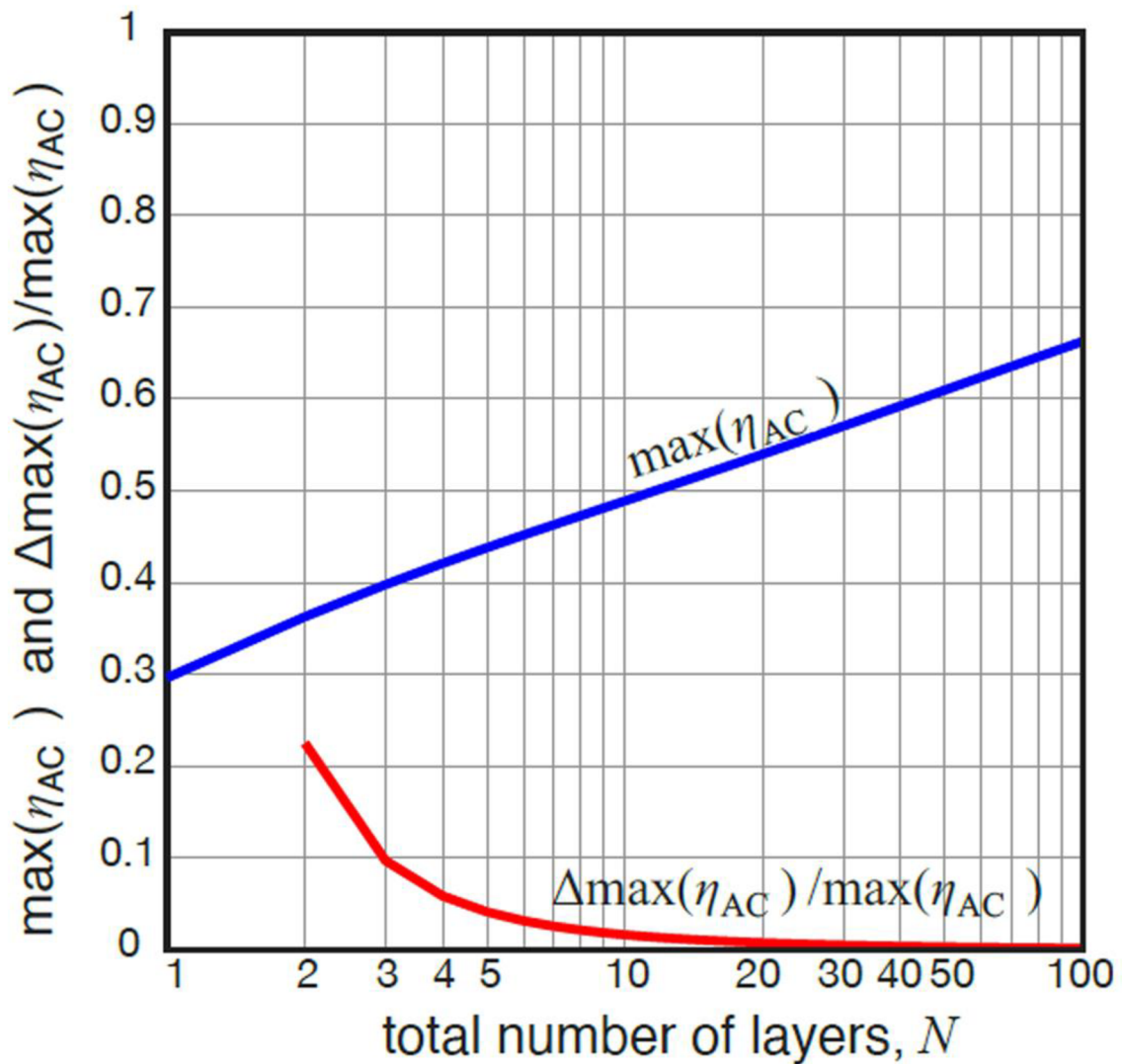


Figure 19: The maximal ACE as a function of N (plotted on a log scale). Although $\max(\eta_{AC})$ increases with increasing N , the relative ACE increase, $\Delta \max(\eta_{AC}) / \max(\eta_{AC})$, becomes small for $N > 5$ and negligible for $N > 10$

As indicated in the theory section, the Steiros2018 model is one of many models, published over 80 years that provide a fluid mechanical formulation for the filtered fraction (theory section). The functional form, as well as the asymptotic behavior of the filtered fraction predicted by alternative theories, varies substantially (Figure 20A).

In that respect, the Glauert1932 [116] model and the Rivera2011 [19] model represent two extreme behaviors, while the Steiros2018 model adopted here and its precursor, the Koo1973 model, are intermediate for the limiting behavior of φ as $s \rightarrow 0$. The prediction of the models for small solidity is especially important in the context of multi-layer collectors since their maximal ACE is attained for solid fractions below 0.3 (Figure 20B).

A comparative analysis of the design space for these models is also informative. Notably, although the models disagree on the maximum ACE that can be achieved for a given N , their respective ACE ridges follow similar arcs in design space (Figure 20B). Specifically, they all go through a small target area ($0.25 < s < 0.35$, $N = 4, 5$) where the multi-layer collectors achieve an efficiency $\sim 40\%$ better than the most efficient single-layer collectors. The quantitative agreement between the models shows the robustness of the efficiency optimization in the design space.

Interestingly, the subspace where η_{AC} is locally maximized follows closely curves of constant filtered. Fraction for all four models (Figure 21). Therefore, the improved aerodynamic collection efficiency of multilayer fog collectors comes almost exclusively from improvements in the incident fraction as new layers are added to the system.

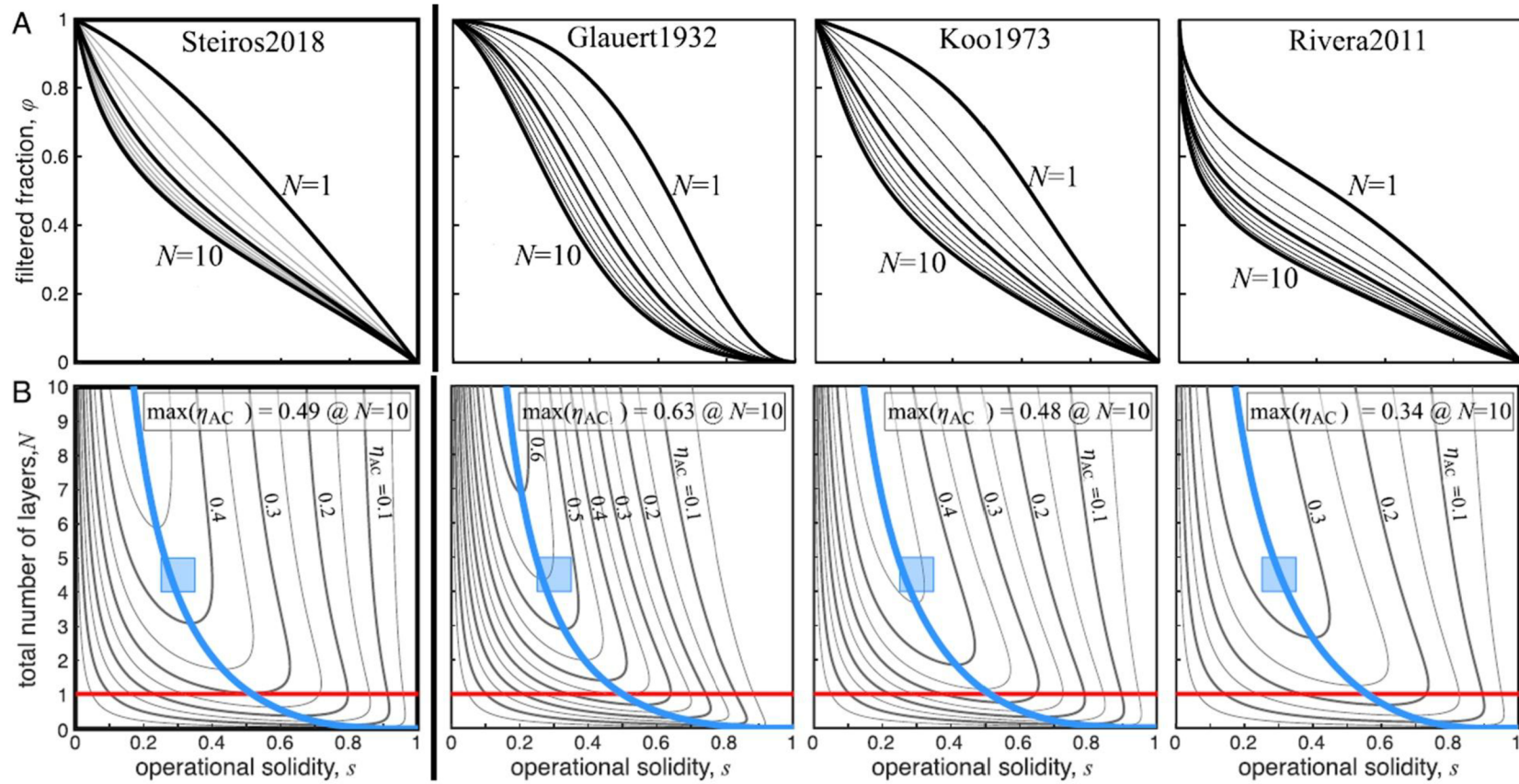


Figure 20: The ACE ridge of four alternative models for the filtered fraction. (A) The filtered fraction of the various models. Note the model-dependent form of the asymptotic behavior of $\varphi(s)$ as $s \rightarrow 0$. (B) Design space for the models listed in A. The blue subspace marks the region within which ACE is locally maximized, either at constant N (lower edge of the blue strip) or at constant s (upper edge of the blue strip). The red square is the suggested target design

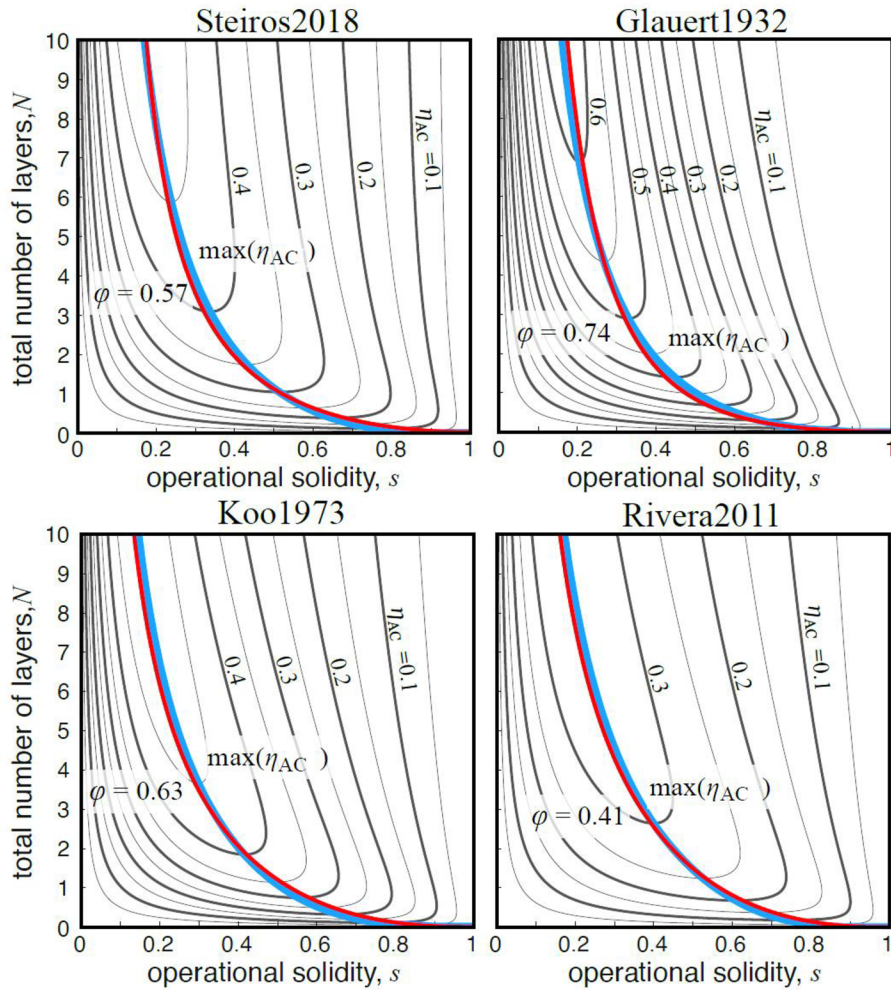


Figure 21: The $\max(\eta_{AC})$ subspace (blue curves) overlaps closely with level curves for the filtered fraction (red) in design space

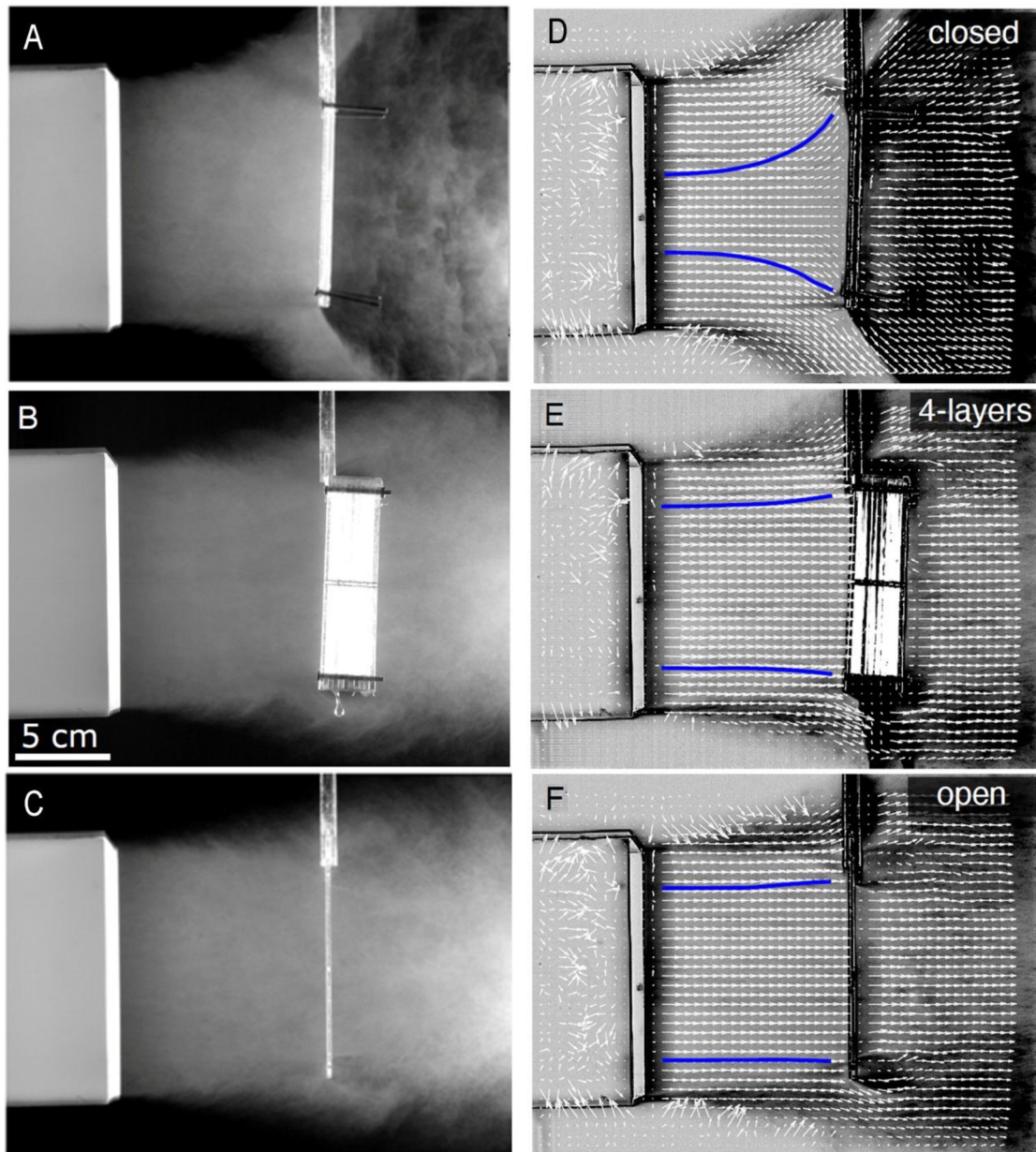


Figure 22: Measurement of ACE for a multi-layer harp collector ($s = 0.17$, $N = 4$). (A) Close-up of the fog jet filtering through a closed collector. (B) Close-up of the fog jet filtering through a 4-layer collector. (C) Close-up of the fog jet filtering through an open collector. (E) Fog flows around a closed collector. (E), a 4-layer harp (F), and an open frame. The blue curves indicate streamlines

Because the models differ substantially in their predicted max ACE (from 34% to 63% for a 10-layer collector), we undertook a series of experimental observations to quantify the effective efficiency of multilayer collectors. As noted above, the equation for η_{AC} is first and foremost a statement about two geometrical ratios: the area ratio associated with the filtered fraction and the solidity s of the mesh (ratio of the obstructed area over the total area of one collector layer).

To assess the ACE, we developed a wind tunnel to produce realistic fog conditions in the laboratory (Figure 10). Experimenting with four-layer harp collector ($l = 100$ mm, $h = 2$ mm, $d = 0.150$ mm), we found an operating solidity of $s = 0.17$ (Figures 23A, B), giving an incident fraction of $\chi = 1 - (1-s)^4 = 0.53$. Integrating the flow field, we arrived at a filtered fraction of $\varphi_{obs} = (l_{\infty} / l)^2 = 0.81 \pm 0.016$ (Figures 24).

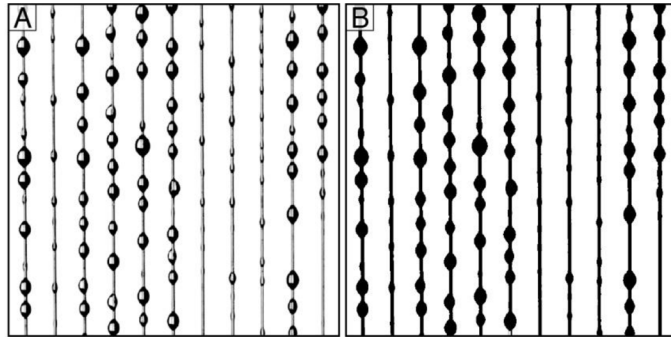


Figure 23: Operational shade coefficient of a simple harp (A) Photo of the mesh under operating conditions. (B) Binary (black/white) version of (A) Used to compute the solidity. The “dry” solidity is 0.075 while the “wet” solidity is 0.17

Based on the measured incident and filtered fractions, the aerodynamics collection efficiency is $\eta_{AC} = \varphi\chi = 43\%$, which exceeds slightly the value of 37% predicted by the Steiros2018 model (Figure 18). The discrepancy arises in part because of the impossibility of measuring the flow field within 10 mm of the collector’s surface with our current experimental setup. The truncated velocity field leads to a slight overestimate of the filtered fraction (Table 3 and Figure 22D-F).

Given the care needed to measure ACE, it might be asked why it should be preferred as a performance standard over the total water collection efficiency, η_{tot} , as defined in Eq. 1. The reason is that although Eq. 1 appears tractable at first sight, a more detailed analysis (Eq. 6) reveals that η_{tot} involves the lost mass fraction, $\int_0^\infty \left(1 - \frac{d_\infty(r)}{d} s\right)^N m(r) dr$, where the terms $d_\infty(r)/d$ and $m(r)$ both depend on the radius of the droplets in the incoming fog. Notably, these two terms give, together, scaling on the order of r^5 (see the Theory section). Therefore, unless the probability density function for the droplet sizes, $f(r)$, is characterized precisely, the total water collection efficiencies are impossible to compare.

Table 3: The filtered fraction, φ , computed as a ratio of areas (l_∞^2/l^2)

Collector	l_∞	l	l_∞^2/l^2
four-layer harp	0.093	0.10	0.82
closed	0.047	0.10	0.21
open	0.096	0.10	0.88

In fact, it could be argued that due to its very nonlinear dependence on r , η_{tot} is virtually useless as a metric for efficiency because of its great sensitivity to the presence of rare but large droplets.

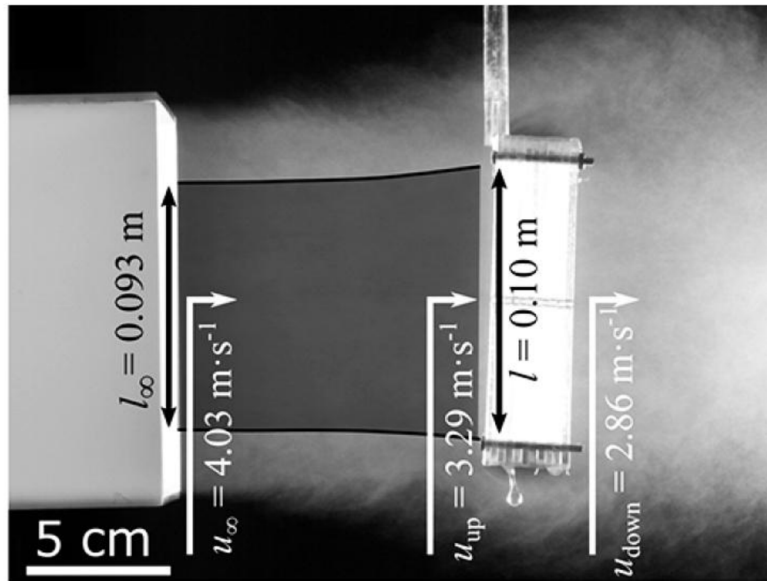


Figure 24: Close-up of the fog jet filtering through the collector with the key variables characterizing the flow field indicated

In contrast, ACE is what is left of η_{tot} when factors affected by the droplet size distribution of fog are eliminated (Eq. 8). Moreover, ACE captures the fundamental trade-off for fog collection. Therefore, in an effort to increase the repeatability and portability of future research in fog collection, we propose the geometrical measurement of ACE as a potential standard for the field (Figure 25).

As a final validation of the performance of multilayer collectors, we compare their yield with that of the standard fog collecting medium—two plies of Raschel mesh (“dry” solidity $s = 0.6$) [77] without spacing between them and thus approximating a single-layer collector. As expected, the yield of the multilayer harps greatly exceeds that of the Raschel standard (Figure 16). Notably, even a single harp layer offers a slightly better yield than the two-ply Raschel mesh (Figure 15A).

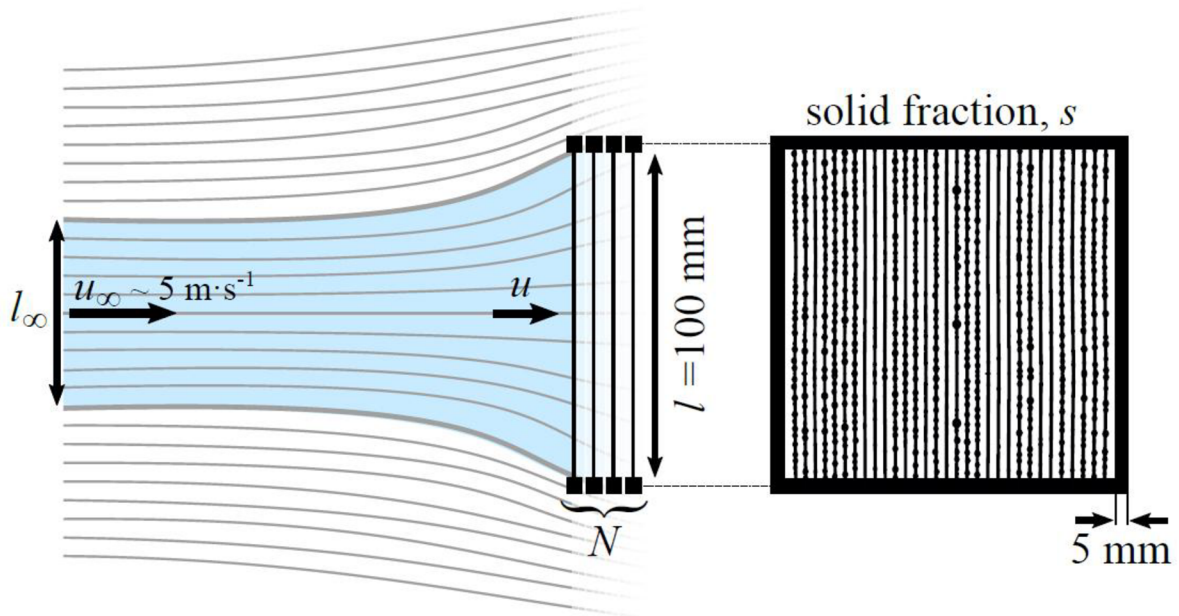


Figure 25: Proposed standard for the measurement of ACE. Prototypes should be square with $100 \text{ mm} \times 100 \text{ mm}$ of open area and a frame of 5 mm on all sides. The operational solid fraction s and the number of layers N are free parameters to be adjusted. The ACE should be measured at a free stream velocity close to $5 \text{ m}\cdot\text{s}^{-1}$ and in the presence of fog

The poor performance of the Raschel mesh under well-defined laboratory conditions is explained by the fact that the two-ply mesh exceeds greatly the optimal operational solidity ($s_{\text{Raschel}} \approx 0.7$ vs $s_{\text{opt}} \approx 0.5$). While the multiharp designs outperform single-layer designs for all N , these collectors lose some of their yield for $N \geq 6$ (Figure 26A), a result that is not predicted from the design space. This efficiency loss probably arises because of the increasing boundary layer that develops in the vicinity of the collector frame.

In the case of a 10-layer collector, the frame depth exceeds 50 mm while the open area for filtration remains $100 \text{ mm} \times 100 \text{ mm}$. In other words, for large N , the collector depth is such that the collector forms an increasingly long tube through which the fog stream must filter. Despite this limitation, the five-layer harp offered a four-fold increase in yield (Figure 26A).

These results were confirmed in field experiments with the 4-layer harp prototype shown in Figure 6A. During a period of low fog, the prototype collected $4.3 \text{ L}\cdot\text{day}^{-1}\cdot\text{m}^{-2}$ while the two-ply Raschel mesh collected only $1 \text{ L}\cdot\text{day}^{-1}\cdot\text{m}^{-2}$ (Figure 26B).

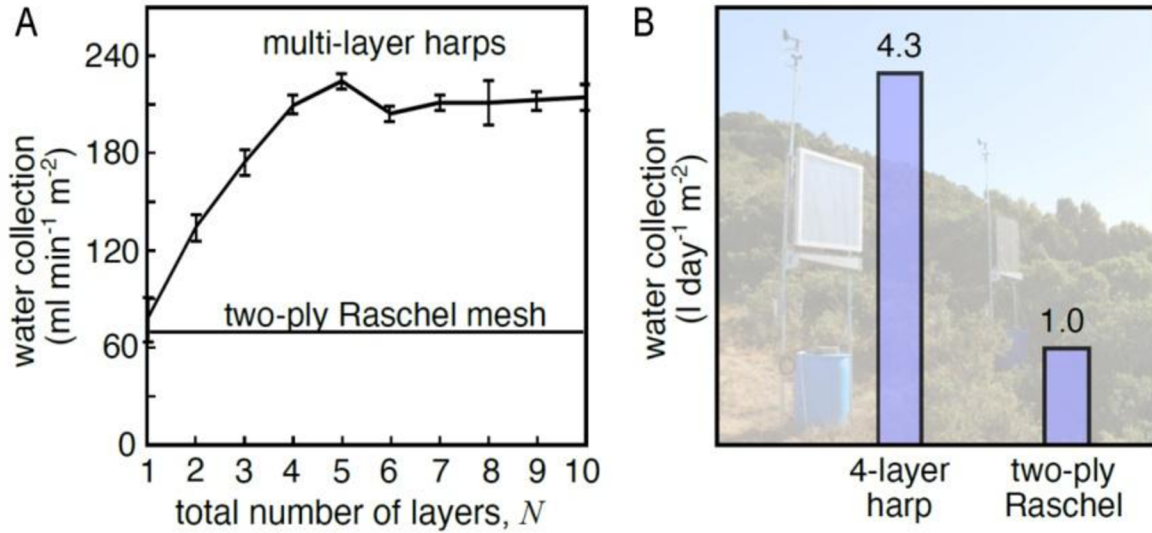


Figure 26: Yield measurements. (A) The yield of multi-layer harps ($1 \leq N \leq 10$, $s = 0.17$, inter-layer spacing of 6 mm) compared to two plies of Raschel mesh with $s = 0.7$ at a fog velocity $u_\infty = 4 \text{ m}\cdot\text{sec}^{-1}$ (B) Field measurements of yield over 20 days

5.2. Wettability of Vertical Harps for Fog Collection

Previously, Rajaram et al. 2016 [16] worked on the coating of Raschel meshes with Teflon, ZnO nanowires, and hydro beads to check the impact of coatings and surface hydrophobicity and found that the resulting modified mesh harvested 50% more water than of untreated Raschel mesh [16]. The movement of water droplets on a surface that is perpendicular to the gravity is quite faster advancing toward the tip along with the thin water boundary as reported in a previous study [117]. Hydrophilic mesh captured tiny droplets of fog efficiently with more affinity and transports to the tip of collector elements [42, 118].

In a contradiction, Ju et al. described that the hydrophobic surface provides a high growth rate to droplets and rolled them off [119]. Thus, the droplets clung to such surfaces do not spread easily [11]. Similarly, Garrod et al. reported that the hydrophobic surface of mesh harvested more fog than the hydrophilic [120]. Additionally, the surface should have enough adhesion force to collect the fog droplets along with the faster transport to the bottom of the mesh in its vertical orientation. The most favorable condition for an ideal collector element is to provide a free surface for the rebirth of fog droplets and drain them by gravitational force without clogging [23, 121].

For the hydrophobic surfaces, Wenzel and Cassie-Baxter's models showed how surface roughness can affect a water droplet's contact angle. In the Wenzel model, there are no air bubbles underneath the droplet and the droplet is in complete contact with the surface. The droplet sticks very well to the surface and it's called a pinned droplet. Therefore, the surface roughness quantifies by " r ", which is the real surface area divided by the projected surface area. Since every surface has some sort of roughness because no surface is completely smooth at the molecular level. It is assumed that $r > 1$. The Wenzel model states that $\cos \theta^*$ (apparent contact angle) is equal to r times $\cos \theta_E$ (equilibrium contact angle). In this state, water droplets will bounce or roll off. This is useful for water repellent and self-cleaning surfaces [122, 123].

Herein, we applied Silane coating on our prototype to make it hydrophobic. It provides low surface energy to the droplets on the surface of FCE and compels them to roll down rapidly. The component that imparts the capacity of an organosilane to create a hydrophobic surface is silane allocation on the surface, organic substitution, remaining unreacted groups of the silane and the amount of surface coverage. The organic substitution should be non-polar to create a hydrophobic surface.

The hydrophobic impact of the organic substitution may associate with the free energy of shifting hydrocarbon molecules from the aqueous state to the uniform hydrocarbon state. The plasma treatment incorporates hydroxyl group to enhance the water affinity while silane eliminates the hydroxyls as water adsorbing sites and supplies anchor positions for the non-polar organic substitution, which defends the polar entities from water interaction [87].

The hydrophilic-hydrophobic patterned surface by the inspiration of the Namibian beetle has been illustrated by many bioinspired designs. The design allows the moisture to be collect by hydrophilic bumps or trichomes on the hydrophobic surface with the strong driving force to drain water [124, 125].

6.2.1. Characterization

Static contact angle

Static contact angle evaluation of untreated and treated (hydrophilic and hydrophobic) samples was determined with a goniometer system (Kruss Easy Drop) using $0.5 \mu\text{l}$ (micro litter) of water drop and enlist the results as shown in Figure 27.

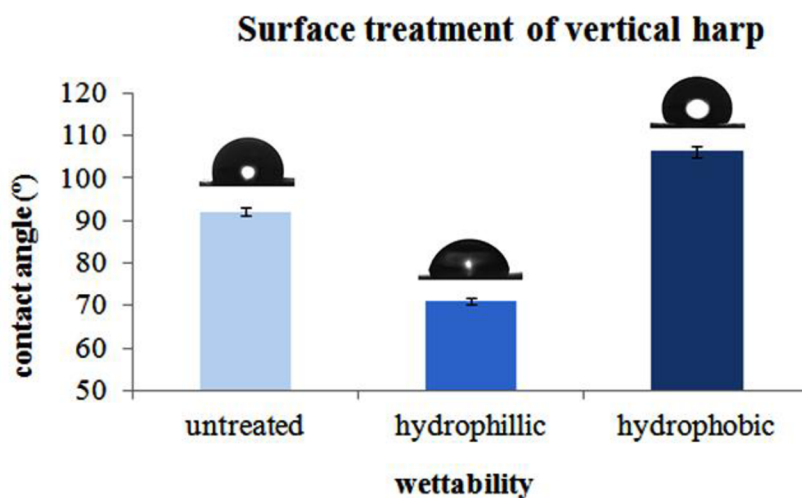


Figure 27: Contact angle results of untreated, hydrophilic surfaces and hydrophobic surfaces

To calculate the yield, the untreated monofilament sample and treated samples with hydrophilic and hydrophobic surfaces were hung at a distance of 10 mm from the head of the fog generator for 30 minutes (Figure 12). The fog droplets were intercepted by the hanging samples and saved in a funnel guiding to a cylinder. The given results are shown in Figure 28. It is determined that the specimen with surface roughness and hydrophilic behavior presented a

decline in fog collection in comparison with the untreated sample while the hydrophobic surface collected more water as shown in Figure 28. Indeed, distinct nature of the hydrophilic surface structure, the droplets coalesce on the hydrophilic spots and expand in volume, but do not leave until they attain a specific size, subject to the proportion and gravity, which decelerates the water collection dynamics. This behavior restricts the deposition of new incoming fog droplets on the monofilament [11]. On the other hand, the hydrophobic surface of the sample provides fast detachment from the surface due to weak solid-liquid interaction rather than the growth of water droplets. Eventually, the tiny droplets initiate to roll down on the tilted hydrophobic surface to the storage. Such structures have been utilized for the drag reduction in attribute to reduce the ability of contact angle between the surface and water droplet (surface wetted area) [126].

The droplet mobility on the hydrophobic surface depends on the WCA, direction of the droplet's movement, the surface morphology of the collector element, and physical characteristics of the droplet. A supplementary aspect that obscures this problem is the droplet pinning to some local sites which is hard to calculate precisely. It should take into account, absence of pinning effects, a theoretical method can be applied to determine contact angle hysteresis and the force of detachment from a single fiber [127].

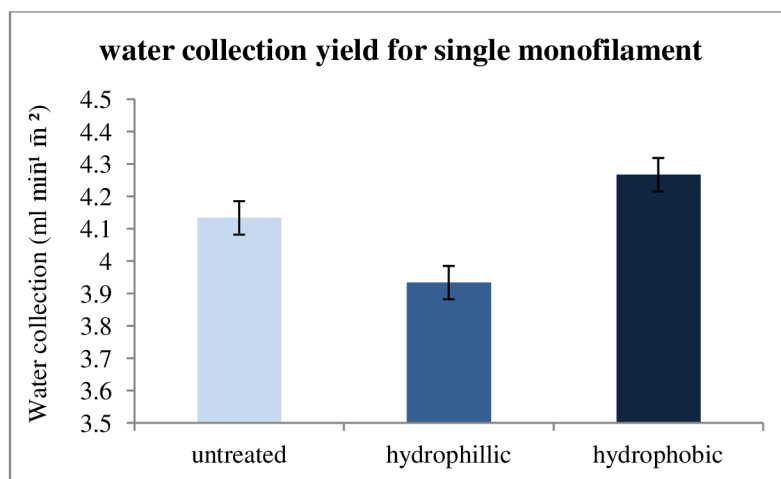


Figure 28: Water collection yield for single monofilament of all three samples

It is specified that our hydrophobic monofilament sample does not demonstrate any substantial clogging as the hydrophilic monofilament sample does. The basic aim of surface modification was always to enhance the deposition of fog droplets and rapid transport to drainage.

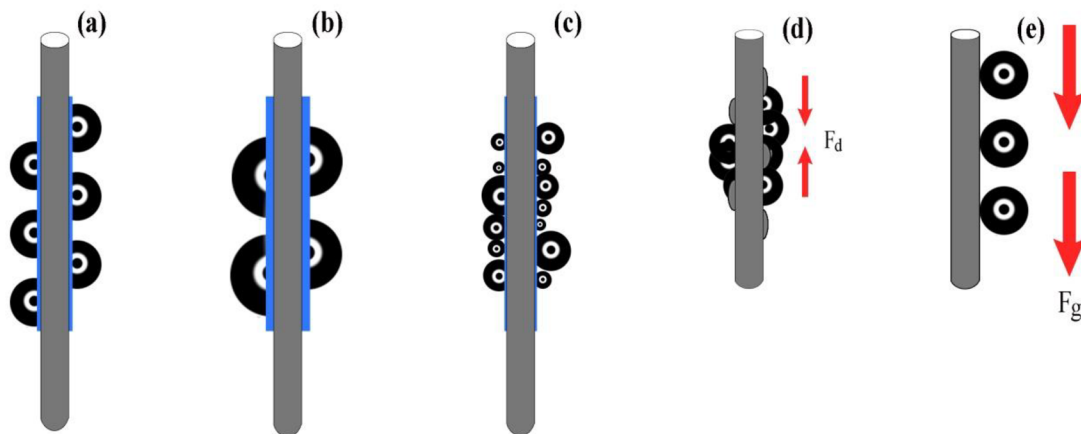


Figure 29: Display the position and shape of water droplets on the samples. (a) Illustration of fog on the untreated filament before slide down. (b) Demonstration of captured droplet areas of hydrophilic filament in the same length segment as an original filament with droplet area. (c) A bunch of small fog droplets adsorbs on the hydrophobic surface before it starts to roll down. (d) Driving force (F_d) produces a wettability slope of droplets on the surface of vertical FCEs dealt with plasma treatment. (e) The fog droplets grown on the hydrophobic surface approach the significant sliding volume and rapidly move along the vertical path with the force of gravity (F_g)

Generally, plasma treatment incorporates new oxygen-containing groups on polymer surfaces to contribute to the hydrophilicity [89] that leads to clinging the fog droplets for a long time. The coalesce of tiny droplets makes its size bigger on all sides of the tubular collector element (Figure 31a). Wetting also creates the water film around the surface which enhances the affinity of droplets to collector samples. Meanwhile, the hydrophobic surface rolls down the droplets on which portion of the surface it is born as shown in Figure 31b.

AFM images of untreated and air-treated DBD plasma of PE monofilaments are shown in Figure 30. Dry air plasma-treated sample observed with small bumps on the surface extracting

as surface roughness. This surface is supposed to catch oxygen-functionalities on the polymer chains and reduced the contact angle up to the saturated region [128].

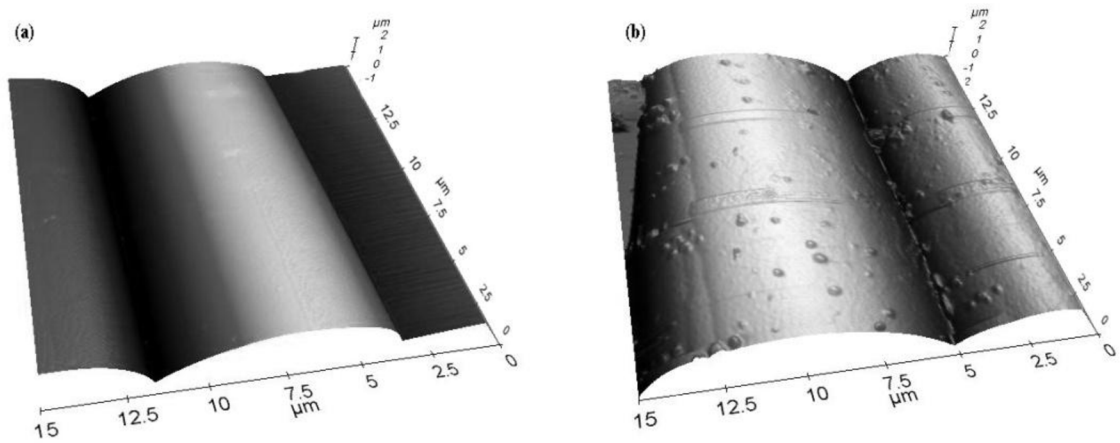


Figure 30: AFM images of (a) untreated and (b) dry air plasma treated PE monofilament samples

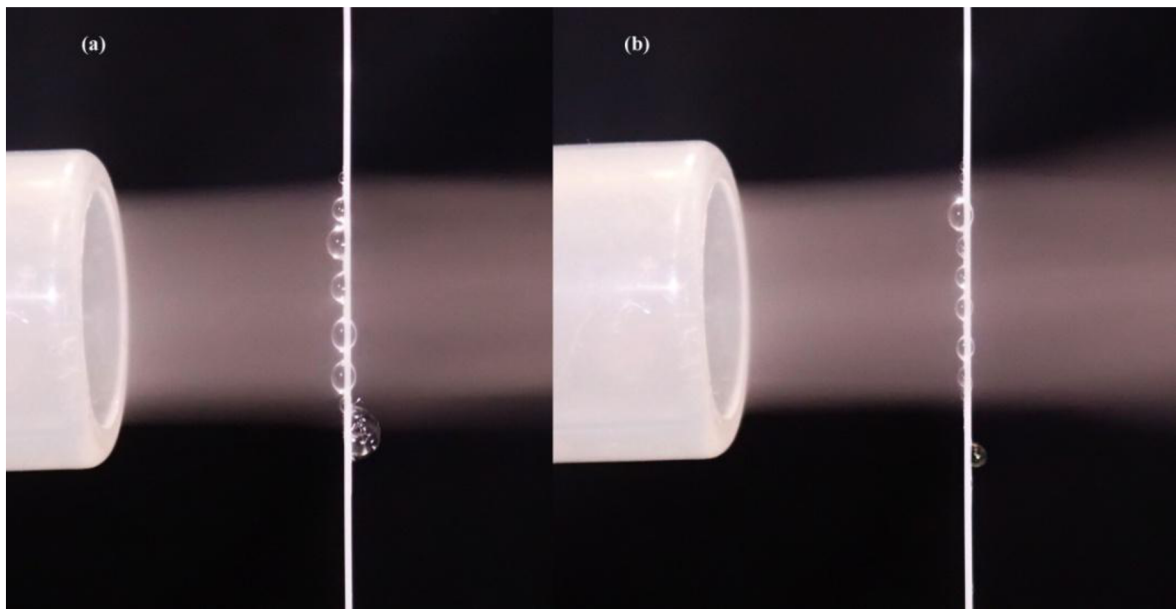


Figure 31: Deposition and adhesion of droplets to the monofilament. In (a), hydrophilic surface bond with droplet and provide enough time to make it bigger until it forces of gravity overcomes the weight of the droplet. In (b), the hydrophobic surface does not allow the droplets to be stayed there for a longer time and compel the droplets to roll down

Contact angle hysteresis

The main purpose of adding the hydrophobic coatings to the FCE are to minimize the CAH of the droplets clung to the surface and hence transport to drainage. This effect also helps to understand why we keep the diameter of the collector element minimum. As described in previous studies [129, 130], the pinning force is caused by the formation of CAH. A droplet on a collector element may be in the barrel form or cling on the side of the collector element [131]. Herein, we observed both states for the falling droplets, but in the flow trajectory, it was clung on the side of the collector element as shown in Figure 31 (a,b). Moreover, the contraction in the size of droplets may be attributed to the reduction in pinning force that is linked with CAH as described in the following equation [132]:

$$f_p = -\sigma w(\cos\theta_r - \cos\theta_a) \quad (15)$$

Here f_p is the pinning force, σ is the surface tension and w is the width of the droplet while the minus symbol indicates the inverse direction of pinning force from the droplet flow. The reduction in CAH is attributed to the presence of hydrophobicity which may tend to the depinning of the surface contact and rapid shedding of droplets.

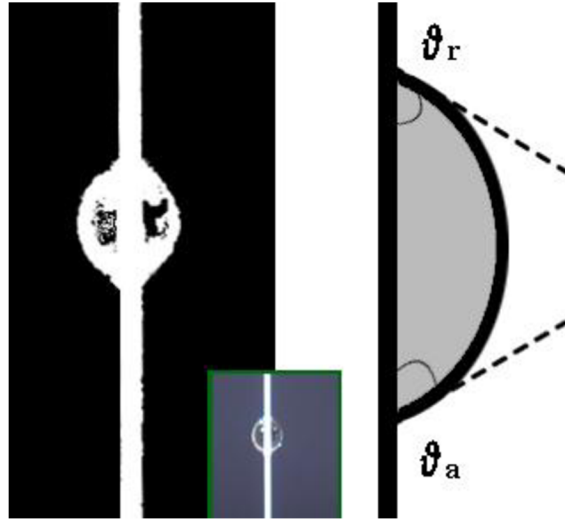


Figure 32: A water droplet on a vertical surface of fog collector element, caught at the critical advancing angle (θ_a) and the critical receding angle (θ_r).

It is quite hard to measure the CAH experimentally even on smooth surfaces. This calculation is generally in between the receding (θ_r) and advancing (θ_a) angles. The difference of both angles is empirically expressed as; $CAH = \theta_a - \theta_r$. As demonstrated in Figure 32, the CAH of untreated PE monofilament was about 6.2° while 7.6° and 5.1° was the measure for hydrophilic and hydrophobic surface respectively. It is seen that the CAH provided the most optimum stable level to encounter the gravitational force. It is also confined that the untreated surface exhibited the lowest hysteresis as compared to the hydrophilic surface. The contradictory, hydrophobic sample showed the lowest hysteresis in comparison with the untreated sample.

Droplets impaction to the fog collector element?

A stream of fog droplets hit each element of the fog collector and some of them are caught by the collector's element while others bypass the structure as shown in figure 33.

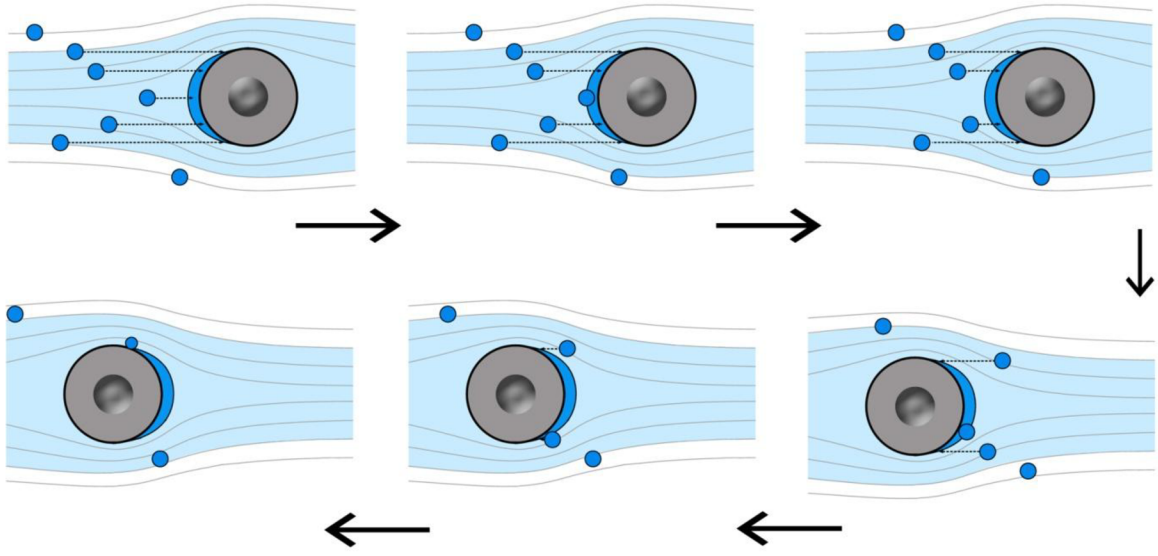


Figure 33: Droplets impaction on the fog collector element

7. Conclusions and Future Work

In this research work, we have presented designs for optimally efficient passive fog collectors by focusing on a geometrical relation (Eq. 8) known as the aerodynamic collection efficiency (ACE). As we have shown, the maximal values of ACE are achieved only through the use of multilayer collectors whose efficiency can exceed 40% that of the best single-layer collectors. The analysis shows that taking into account the most effective use of materials, the optimal fog collector has $N = 4, 5$ layers and operating solidity $s = 0.3 \pm 0.05$, assuming that the operating thread diameter is sufficiently small to maximize inertial impaction of fog droplets. These conclusions were validated experimentally for multilayer harp collectors. When optimized, the latter can collect as much as four times that collected by the standard two-ply Raschel mesh, both under laboratory and field conditions.

Nowadays, researchers are specifically working on fog collection efficiency with surface modification methods to provide the droplets quick transportation and rolled them off to storage [119, 120, 125]. In our study, the FCE with hydrophobic treatment slightly improved the yield and efficiency of a multilayer fog collector. The major parameter is the structural design of the collector which enhances the productivity of the mechanism. The water collection yield of a single monofilament was enhanced by 107% by incorporating hydrophobic coating on the vertical collector elements. It is not possible to enhance the water collection yield by hydrophilic plasma treatment due to the clinging of fog droplets for a longer time and restrict the path of new coming droplets to be grown on the collector surface. These findings show that surface hydrophobicity developed a slight modification on the surface and does prompt the process a little efficiently. In this fog harvesting study, we conclude that the water collection efficiency is mainly coupled with the design of the collection. This study could help to develop a large-scale fog harp that would be cost-effective and easy to install for fog harvesting. The manifestations of CAH enforced our results to include the hydrophobic coating for an efficient fog collection rate.

In the future, the mass production of multilayer harps would be much more efficient to collect the high yield of fog collection. Moreover; a parabolic fog collector could be more appropriate to catch a maximum fraction of fog particles.

8. References

- [1] U. Water, "Sustainable Development Goal 6 synthesis report on water and sanitation," *Published by the United Nations New York, New York*, vol. 10017, 2018.
- [2] J. K. Domen, W. T. Stringfellow, M. K. Camarillo, and S. Gulati, "Fog water as an alternative and sustainable water resource," *Clean Technologies and Environmental Policy*, vol. 16, pp. 235-249, 2014.
- [3] C. Schunk, P. Trautwein, H. Hruschka, E. Frost, L. Dodson, A. Derhem, *et al.*, "Testing water yield, efficiency of different meshes and water quality with a novel fog collector for high wind speeds," *Aerosol and Air Quality Research*, vol. 18, pp. 240-253, 2018.
- [4] D. Beysens, *Dew Water*: River Publishers, 2018.
- [5] K. F. Kaseke and L. Wang, "Fog and dew as potable water resources: Maximizing harvesting potential and water quality concerns," *GeoHealth*, vol. 2, pp. 327-332, 2018.
- [6] K. Gerasopoulos, W. L. Luedeman, E. Ölçeroglu, M. McCarthy, and J. J. Benkoski, "Effects of engineered wettability on the efficiency of dew collection," *ACS applied materials & interfaces*, vol. 10, pp. 4066-4076, 2018.
- [7] H. Kim, S. Yang, S. R. Rao, S. Narayanan, E. A. Kapustin, H. Furukawa, *et al.*, "Water harvesting from air with metal-organic frameworks powered by natural sunlight," *Science*, vol. 356, pp. 430-434, 2017.
- [8] R. Schemenauer and P. Cereceda, "Fog-water collection in arid coastal location," *AMBIO*, vol. 20, pp. 303-308, 1991.
- [9] R. S. Schemenauer and P. Cereceda, "Fog collection's role in water planning for developing countries," in *Natural resources forum*, 1994, pp. 91-100.
- [10] O. Klemm, R. S. Schemenauer, A. Lummerich, P. Cereceda, V. Marzol, D. Corell, *et al.*, "Fog as a fresh-water resource: overview and perspectives," *Ambio*, vol. 41, pp. 221-234, 2012.
- [11] K.-C. Park, S. S. Chhatre, S. Srinivasan, R. E. Cohen, and G. H. McKinley, "Optimal design of permeable fiber network structures for fog harvesting," *Langmuir*, vol. 29, pp. 13269-13277, 2013.
- [12] D. Cruzat and C. Jerez-Hanckes, "Electrostatic fog water collection," *Journal of Electrostatics*, vol. 96, pp. 128-133, 2018.

- [13] M. Damak and K. K. Varanasi, "Electrostatically driven fog collection using space charge injection," *Science advances*, vol. 4, p. eaao5323, 2018.
- [14] R. Holmes, J. de Dios Rivera, and E. de la Jara, "Large fog collectors: New strategies for collection efficiency and structural response to wind pressure," *Atmospheric research*, vol. 151, pp. 236-249, 2015.
- [15] Y. Jiang, S. Savarirayan, Y. Yao, and K.-C. Park, "Fog collection on a superhydrophilic wire," *Applied Physics Letters*, vol. 114, p. 083701, 2019.
- [16] M. Rajaram, X. Heng, M. Oza, and C. Luo, "Enhancement of fog-collection efficiency of a Raschel mesh using surface coatings and local geometric changes," *Colloids and Surfaces A: Physicochemical and Engineering Aspects*, vol. 508, pp. 218-229, 2016.
- [17] W. Shi, M. J. Anderson, J. B. Tulkoff, B. S. Kennedy, and J. B. Boreyko, "Fog harvesting with harps," *ACS applied materials & interfaces*, vol. 10, pp. 11979-11986, 2018.
- [18] L. Zhang, J. Wu, M. N. Hedhili, X. Yang, and P. Wang, "Inkjet printing for direct micropatterning of a superhydrophobic surface: toward biomimetic fog harvesting surfaces," *Journal of Materials Chemistry A*, vol. 3, pp. 2844-2852, 2015.
- [19] J. de Dios Rivera, "Aerodynamic collection efficiency of fog water collectors," *Atmospheric Research*, vol. 102, pp. 335-342, 2011.
- [20] R. Labbé and C. Duprat, "Capturing aerosol droplets with fibers," *Soft Matter*, vol. 15, pp. 6946-6951, 2019.
- [21] H. Andrews, E. Eccles, W. Schofield, and J. Badyal, "Three-dimensional hierarchical structures for fog harvesting," *Langmuir*, vol. 27, pp. 3798-3802, 2011.
- [22] J. Lin, X. Tan, T. Shi, Z. Tang, and G. Liao, "Leaf Vein-Inspired Hierarchical Wedge-Shaped Tracks on Flexible Substrate for Enhanced Directional Water Collection," *ACS applied materials & interfaces*, vol. 10, pp. 44815-44824, 2018.
- [23] M. Azad, D. Ellerbrok, W. Barthlott, and K. Koch, "Fog collecting biomimetic surfaces: Influence of microstructure and wettability," *Bioinspiration & biomimetics*, vol. 10, p. 016004, 2015.
- [24] X. Jing and Z. Guo, "Durable Lubricant-Impregnated Surfaces for Water Collection under Extremely Severe Working Conditions," *ACS applied materials & interfaces*, 2019.

- [25] C. Li, Y. Liu, C. Gao, X. Li, Y. Xing, and Y. Zheng, "Fog Harvesting of a Bioinspired Nanocone-Decorated 3D Fiber Network," *ACS applied materials & interfaces*, vol. 11, pp. 4507-4513, 2019.
- [26] R. LeBoeuf and E. de la Jara, "Quantitative goals for large-scale fog collection projects as a sustainable freshwater resource in northern Chile," *Water international*, vol. 39, pp. 431-450, 2014.
- [27] D. H. Benzing and K. M. Burt, "Foliar permeability among twenty species of the Bromeliaceae," *Bulletin of the Torrey Botanical Club*, pp. 269-279, 1970.
- [28] P. W. Rundel, B. Palma, M. Dillon, M. R. Sharifi, E. Nilsen, and K. Boonpragob, "Tillandsia landbeckii in the coastal Atacama Desert of northern Chile," *Revista chilena de historia natural*, vol. 70, pp. 341-349, 1997.
- [29] P. S. Raux, S. Gravelle, and J. Dumais, "Design of a unidirectional water valve in Tillandsia," *Nature communications*, vol. 11, pp. 1-7, 2020.
- [30] C. Gischler, "The missing link in a production chain. Vertical obstacles to catch Camanchaca," 1991.
- [31] C. M. Regalado and A. Ritter, "The design of an optimal fog water collector: A theoretical analysis," *Atmospheric Research*, vol. 178, pp. 45-54, 2016.
- [32] M. M. Mekonnen and A. Y. Hoekstra, "Four billion people facing severe water scarcity," *Science advances*, vol. 2, p. e1500323, 2016.
- [33] T. M. Boers and J. Ben-Asher, "A review of rainwater harvesting," *Agricultural water management*, vol. 5, pp. 145-158, 1982.
- [34] J. de Dios Rivera and D. Lopez-Garcia, "Mechanical characteristics of Raschel mesh and their application to the design of large fog collectors," *Atmospheric research*, vol. 151, pp. 250-258, 2015.
- [35] F. D. Eckardt and R. S. Schemenauer, "Fog water chemistry in the Namib Desert, Namibia," *Atmospheric Environment*, vol. 32, pp. 2595-2599, 1998.
- [36] C. Escobar, A. Lopez, H. Aristizabal, and J. Molina, "Operational fog collection and its role in environmental education and social reintegration: A case study in Colombia," in *5th International Conference on Fog, Fog Collection and Dew, held 25-30 July, 2010 in Münster, Germany*. <http://www.fogconference.org>, id. FOGDEW2010-67, 2010.

- [37] S. Algarni, "Assessment of fog collection as a sustainable water resource in the southwest of the Kingdom of Saudi Arabia," *Water and environment journal*, vol. 32, pp. 301-309, 2018.
- [38] R. S. Schemenauer and P. Cereceda, "Fog-water collection in arid coastal locations," *IV Reunión Nacional sobre sistemas de Captación de lluvia*, p. 279, 2012.
- [39] R. S. Schemenauer and P. Cereceda, "Fog-water collection in arid coastal locations," *Ambio*, pp. 303-308, 1991.
- [40] M. Azeem, A. Guérin, T. Dumais, L. Caminos, R. E. Goldstein, A. Pesci, *et al.*, "Optimal Design of Multi-Layer Fog Collectors," *ACS Applied Materials & Interfaces*, 2020.
- [41] R. Schemenauer, "Potential for log water collection in the Dhofar region of southern Oman," *Report to the World Meteorological Organization, Technical Coordination Division*, 1989.
- [42] M. Azeem, A. Boughattas, J. Wiener, and A. Havelka, "Mechanism of liquid water transport in fabrics; A review," *Fibres and Textiles*, vol. 24, pp. 58-65, 2017.
- [43] B. S. Lalia, S. Anand, K. K. Varanasi, and R. Hashaikeh, "Fog-harvesting potential of lubricant-impregnated electrospun nanomats," *Langmuir*, vol. 29, pp. 13081-13088, 2013.
- [44] M. Cao, J. Xiao, C. Yu, K. Li, and L. Jiang, "Hydrophobic/hydrophilic cooperative Janus system for enhancement of fog collection," *Small*, vol. 11, pp. 4379-4384, 2015.
- [45] R. Ghosh, T. K. Ray, and R. Ganguly, "Cooling tower fog harvesting in power plants—A pilot study," *Energy*, vol. 89, pp. 1018-1028, 2015.
- [46] M. Azad, T. Krause, L. Danter, A. Baars, K. Koch, and W. Barthlott, "Fog collection on polyethylene terephthalate (PET) Fibers: influence of cross section and surface structure," *Langmuir*, vol. 33, pp. 5555-5564, 2017.
- [47] F. J. Tan, M. A. P. Estanislao, A. M. A. Gregorio, and I. J. D. Navea, "The potential of fog harvesting in tropical highlands as an alternative water resource: the case of Atok, Benguet, Philippines," in *E3S Web of Conferences*, 2019.
- [48] E. Shanyengana, J. Henschel, M. Seely, and R. Sanderson, "Exploring fog as a supplementary water source in Namibia," *Atmospheric Research*, vol. 64, pp. 251-259, 2002.
- [49] O. Al- Jayyousi and M. Mohsen, "Evaluation of fog collection in Jordan," *Water and Environment Journal*, vol. 13, pp. 195-199, 1999.

- [50] M. Mileta and Z. Likso, "Fog water collection with SFC on the mountain Velebit (Croatia) during the period 2000–2009," in *Proceedings of the 5th International Conference on Fog, Fog Collection and Dew*, 2010.
- [51] R. S. Schemenauer, P. Osses, and M. Leibbrand, "Fog collection evaluation and operational projects in the Hajja Governorate, Yemen," in *Proceedings of the Third International Conference on Fog, Fog Collection and Dew*, 2004.
- [52] M. Rosato, F. Rojas, and R. Schemenauer, "Not just beneficiaries: Fostering participation and local management capacity in the Tojquia fog-collection project, Guatemala," in *Proceedings of the 5th International Conference on Fog, Fog Collection and Dew*, 2010.
- [53] J. Olivier and C. De Rautenbach, "The implementation of fog water collection systems in South Africa," *Atmospheric Research*, vol. 64, pp. 227-238, 2002.
- [54] S. A. Abdul-Wahab, A. M. Al-Damkhi, H. Al-Hinai, K. A. Al-Najar, and M. S. Al-Kalbani, "Total fog and rainwater collection in the Dhofar region of the Sultanate of Oman during the monsoon season," *Water International*, vol. 35, pp. 100-109, 2010.
- [55] S. A. Abdul-Wahab, H. Al-Hinai, K. A. Al-Najar, and M. S. Al-Kalbani, "Feasibility of fog water collection: a case study from Oman," *Journal of Water Supply: Research and Technology—AQUA*, vol. 56, pp. 275-280, 2007.
- [56] M. R. S. Price, A. Al-Harthy, and R. Whitcombe, "Fog moisture and its ecological effects on Oman," *Arid lands: today and tomorrow*, pp. 69-88, 1988.
- [57] R. S. Schemenauer and P. Cereceda, "Water from fog covered mountains," *Waterlines*, vol. 10, no. 4, 1992.
- [58] B. Henderson and D. Falk, "Fog water collection in ecuador: An appropriate technology for the rural poor," in *Proceedings of the 2nd International Conference on Fog and Fog Collection*, 2001.
- [59] M. Marzol, J. Sanchez Megía, A. Yanes, J. Bargach, and A. Derhem, "Meteorological Patterns and Fog Water in the Canary Islands and Morocco," in *5th International Conference on Fog, Fog Collection and Dew, held 25-30 July, 2010 in Münster, Germany*. <http://www.fogconference.org>, id. FOGDEW2010-31, 2010.
- [60] M. V. M. Jaen, "Fog water collection in a rural park in the Canary Islands (Spain)," *Atmospheric Research*, vol. 64, pp. 239-250, 2002.

- [61] P. Gandhidasan and H. I. Abualhamayel, "Fog collection as a source of fresh water supply in the Kingdom of Saudi Arabia," *Water and Environment Journal*, vol. 21, pp. 19-25, 2007.
- [62] R. S. Schemenauer and P. Cereceda, "The use of fog for groundwater recharge in arid regions," in *International Seminar on Groundwater and the Environment in Arid and Semiarid Areas, Beijing, China*, 1992, pp. 84-91.
- [63] P. Cereceda, H. Larrain, P. Osses, M. Farías, and I. Egaña, "The spatial and temporal variability of fog and its relation to fog oases in the Atacama Desert, Chile," *Atmospheric Research*, vol. 87, pp. 312-323, 2008.
- [64] R. S. Schemenauer and P. Cereceda, "A proposed standard fog collector for use in high-elevation regions," *Journal of Applied Meteorology*, vol. 33, pp. 1313-1322, 1994.
- [65] R. S. Schemenauer and P. I. Joe, "The collection efficiency of a massive fog collector," *Atmospheric Research*, vol. 24, pp. 53-69, 1989.
- [66] N. D. F. R. Dos Anjos, "Source book of alternative technologies for freshwater augmentation in Latin America and the Caribbean," *International Journal of Water Resources Development*, vol. 14, pp. 365-398, 1998.
- [67] S. A. Abdul- Wahab and V. Lea, "Reviewing fog water collection worldwide and in Oman," *International Journal of Environmental Studies*, vol. 65, pp. 487-500, 2008.
- [68] C. Gischler, "The missing link in a production chain. Vertical obstacles to catch Camanchaca," 2018.
- [69] R. S. Schemenauer and P. Cereceda, "The role of wind in rainwater catchment and fog collection," *Water International*, vol. 19, pp. 70-76, 1994.
- [70] R. S. Schemenauer, H. Fuenzalida, and P. Cereceda, "A neglected water resource: The Camanchaca of South America," *Bulletin of the American Meteorological Society*, vol. 69, pp. 138-147, 1988.
- [71] R. S. Schemenauer, P. Cereceda, and P. Osses, "FogQuest: Fog water collection manual," 2005.
- [72] E. Shanyengana, R. Sanderson, M. Seely, and R. Schemenauer, "Testing greenhouse shade nets in collection of fog for water supply," *Journal of Water Supply: Research and Technology-Aqua*, vol. 52, pp. 237-241, 2003.

- [73] E. Bresci, "Wake characterization downstream of a fog collector," *Atmospheric research*, vol. 64, pp. 217-225, 2002.
- [74] E. L. Petersen, N. G. Mortensen, L. Landberg, J. Højstrup, and H. P. Frank, "Wind power meteorology. Part I: Climate and turbulence," *Wind Energy: An International Journal for Progress and Applications in Wind Power Conversion Technology*, vol. 1, pp. 25-45, 1998.
- [75] R. S. Schemenauer and G. Isaac, "The importance of cloud top lifetime in the description of natural cloud characteristics," *Journal of climate and applied meteorology*, vol. 23, pp. 267-279, 1984.
- [76] J. Jiusto, "Fog structure in clouds: their formation, optical properties and effects'," ed: Academic Press, 1981.
- [77] R. S. Schemenauer and P. Cereceda, "A proposed standard fog collector for use in high-elevation regions," *Journal of Applied Meteorology and Climatology*, vol. 33, pp. 1313-1322, 1994.
- [78] T. S. Glickman and W. Zenk, *Glossary of meteorology*: AMS (American Meteorological Society), 2000.
- [79] M. Ćurić and D. Janc, "On the sensitivity of the continuous accretion rate equation used in bulk-water parameterization schemes," *Atmospheric research*, vol. 39, pp. 313-332, 1995.
- [80] M. Azeem, J. Wiener, and M. Z. Khan, "Hydrophobic analysis of nano-filament polyester fabric," *Vlákna a Textil*, vol. 25, p. 5, 2018.
- [81] A. Salam, M. Q. Khan, T. Hassan, N. Hassan, A. Nazir, T. Hussain, *et al.*, "In-vitro assessment of appropriate hydrophilic scaffolds by co-electrospinning of poly (1, 4 cyclohexane isosorbide terephthalate)/polyvinyl alcohol," *Scientific Reports*, vol. 10, pp. 1-9, 2020.
- [82] M. Azeem, A. Guérin, T. Dumais, L. Caminos, R. E. Goldstein, A. I. Pesci, *et al.*, "Optimal Design of Multilayer Fog Collectors," *ACS applied materials & interfaces*, vol. 12, pp. 7736-7743, 2020.
- [83] J. Ju, X. Yao, S. Yang, L. Wang, R. Sun, Y. He, *et al.*, "Cactus Stem Inspired Cone-Arrayed Surfaces for Efficient Fog Collection," *Advanced Functional Materials*, vol. 24, pp. 6933-6938, 2014.

- [84] H. Bai, J. Ju, R. Sun, Y. Chen, Y. Zheng, and L. Jiang, "Controlled fabrication and water collection ability of bioinspired artificial spider silks," *Advanced Materials*, vol. 23, pp. 3708-3711, 2011.
- [85] Z. Yu, H. Zhang, J. Huang, S. Li, S. Zhang, Y. Cheng, *et al.*, "Namib desert beetle inspired special patterned fabric with programmable and gradient wettability for efficient fog harvesting," *Journal of Materials Science & Technology*, vol. 61, pp. 85-92, 2021.
- [86] H. Drnovska, L. Lapčák, V. Buršíková, J. Zemek, and A. M. Barros-Timmons, "Surface properties of polyethylene after low-temperature plasma treatment," *Colloid and Polymer Science*, vol. 281, pp. 1025-1033, 2003.
- [87] B. Arkles, "and Silanes," *Gelest Inc., Morrisville, PA*, 2006.
- [88] R. Morent, N. De Geyter, J. Verschuren, K. De Clerck, P. Kiekens, and C. Leys, "Non-thermal plasma treatment of textiles," *Surface and coatings technology*, vol. 202, pp. 3427-3449, 2008.
- [89] M. Azeem, A. Javed, H. Morikawa, M. T. Noman, M. Q. Khan, M. Shahid, *et al.*, "Hydrophilization of Polyester Textiles by Nonthermal Plasma," *Autex Research Journal*, vol. 1, 2019.
- [90] D. Seo, J. Lee, C. Lee, and Y. Nam, "The effects of surface wettability on the fog and dew moisture harvesting performance on tubular surfaces," *Scientific reports*, vol. 6, pp. 1-11, 2016.
- [91] N. K. Kim, D. H. Kang, H. Eom, and H. W. Kang, "Biomimetic fog harvesting surface by photo-induced micro-patterning of zinc-oxide silver hierarchical nanostructures," *Applied Surface Science*, vol. 470, pp. 161-167, 2019.
- [92] H. Liu, W.-Y. Xie, F. Song, X.-L. Wang, and Y.-Z. Wang, "Constructing hierarchically hydrophilic/superhydrophobic ZIF-8 pattern on soy protein towards a biomimetic efficient water harvesting material," *Chemical Engineering Journal*, vol. 369, pp. 1040-1048, 2019.
- [93] D. Gurera and B. Bhushan, "Designing bioinspired conical surfaces for water collection from condensation," *Journal of colloid and interface science*, vol. 560, pp. 138-148, 2020.
- [94] D. Gurera and B. Bhushan, "Optimization of bioinspired conical surfaces for water collection from fog," *Journal of colloid and interface science*, vol. 551, pp. 26-38, 2019.

- [95] X. Wang, J. Zeng, X. Yu, C. Liang, and Y. Zhang, "Water harvesting method via a hybrid superwetable coating with superhydrophobic and superhydrophilic nanoparticles," *Applied Surface Science*, vol. 465, pp. 986-994, 2019.
- [96] H. Eral and J. Oh, "Contact angle hysteresis: a review of fundamentals and applications," *Colloid and polymer science*, vol. 291, pp. 247-260, 2013.
- [97] R. S. Schemenauer and P. Cereceda, "The quality of fog water collected for domestic and agricultural use in Chile," *Journal of Applied Meteorology*, vol. 31, pp. 275-290, 1992.
- [98] J. Olivier and J. Van Heerden, "Implementation of an operational prototype fog water collection system," *Water Research Commission Report*, p. 02, 2002.
- [99] E. Sträter, A. Westbeld, and O. Klemm, "Pollution in coastal fog at Alto Patache, Northern Chile," *Environmental Science and Pollution Research*, vol. 17, pp. 1563-1573, 2010.
- [100] J. Goodman, "The microstructure of California coastal fog and stratus," *Journal of Applied Meteorology*, vol. 16, pp. 1056-1067, 1977.
- [101] A. Ito and K. Garry, "Pressure measurements around a two-dimensional gauze at incidence," *Journal of fluids and structures*, vol. 12, pp. 171-181, 1998.
- [102] D. Gordon, "Numerical calculations on viscous flow fields through cylinder arrays," *Computers & Fluids*, vol. 6, pp. 1-13, 1978.
- [103] C. D. Cooper and F. C. Alley, *Air pollution control: A design approach*: Waveland press, 2010.
- [104] C. Gischler, "The missing link in a production chain. Vertical obstacles to catch Camanchaca.," in *UNESCORO STLAC, Montevideo*, ed. Uruguay, 1991.
- [105] I. Langmuir and K. Blodgett, "Mathematical Investigation of water droplet trajectories; GEC Res," *Lab. Schenectady*, vol. 225, 1945.
- [106] P. Morgan, "Fluid flow through screens of low solidity," *The Aeronautical Journal*, vol. 66, pp. 54-56, 1962.
- [107] G. I. Taylor, "The aerodynamics of porous sheets," *Aeronautical Research Council, Reports and Memoranda*, vol. 2237, pp. 163-176, 1944.
- [108] J.-K. Koo and D. F. James, "Fluid flow around and through a screen," *Journal of Fluid Mechanics*, vol. 60, pp. 513-538, 1973.
- [109] K. Steiros and M. Hultmark, "Drag on flat plates of arbitrary porosity," *Journal of Fluid Mechanics*, vol. 853, 2018.

- [110] B. Eckert and F. Pfluger, "The resistance coefficient of commercial round wire grids," 1942.
- [111] I. E. Idel'Cik, "Memento of the losses of load," *Collection of the Direction of Studies and Research of Electricity of France, Paris: Eyrolles, 1969*, 1969.
- [112] H. Glauert, D. Hirst, and A. Hartshorn, *Induced flow through a partially choked pipe*: HM Stationery Office, 1932.
- [113] G. Taylor, "Air resistance of a flat plate of very porous material," *Aeronautical Research Council, Reports and Memoranda*, vol. 2236, pp. 159-162, 1944.
- [114] S. O'kell, T. Henshaw, G. Farrow, M. Aindow, and C. Jones, "Effects of low- power plasma treatment on polyethylene surfaces," *Surface and interface analysis*, vol. 23, pp. 319-327, 1995.
- [115] J. B. Lynch, P. D. Spence, D. E. Baker, and T. A. Postlethwaite, "Atmospheric pressure plasma treatment of polyethylene via a pulse dielectric barrier discharge: Comparison using various gas compositions versus corona discharge in air," *Journal of applied polymer science*, vol. 71, pp. 319-331, 1999.
- [116] H. Glauert, D. Hirst, and A. Hartshorn, *The induced flow through a partially choked pipe with axis along the wind stream*: HM Stationery Office, 1932.
- [117] R. Kannan, V. Vaikuntanathan, and D. Sivakumar, "Dynamic contact angle beating from drops impacting onto solid surfaces exhibiting anisotropic wetting," *Colloids and Surfaces A: Physicochemical and Engineering Aspects*, vol. 386, pp. 36-44, 2011.
- [118] H. Bai, J. Ju, Y. Zheng, and L. Jiang, "Functional fibers with unique wettability inspired by spider silks," ed: Wiley Online Library, 2012.
- [119] J. Ju, K. Xiao, X. Yao, H. Bai, and L. Jiang, "Bioinspired conical copper wire with gradient wettability for continuous and efficient fog collection," *Advanced Materials*, vol. 25, pp. 5937-5942, 2013.
- [120] R. Garrod, L. Harris, W. Schofield, J. McGettrick, L. Ward, D. Teare, *et al.*, "Mimicking a Stenocara Beetle's back for microcondensation using plasmachemical patterned superhydrophobic– superhydrophilic surfaces," *Langmuir*, vol. 23, pp. 689-693, 2007.
- [121] P.-G. De Gennes, F. Brochard-Wyart, and D. Quéré, *Capillarity and wetting phenomena: drops, bubbles, pearls, waves*: Springer Science & Business Media, 2013.

- [122] R. N. Wenzel, "Resistance of solid surfaces to wetting by water," *Industrial & Engineering Chemistry*, vol. 28, pp. 988-994, 1936.
- [123] A. Cassie and S. Baxter, "Wettability of porous surfaces," *Transactions of the Faraday society*, vol. 40, pp. 546-551, 1944.
- [124] E. Qasemi, M. Mahdavinejad, M. Aliabadi, and A. Zarkesh, "Leaf venation patterns as a model for bioinspired fog harvesting," *Colloids and Surfaces A: Physicochemical and Engineering Aspects*, vol. 603, p. 125170, 2020.
- [125] L. T. Nguyen, Z. Bai, J. Zhu, C. Gao, X. Liu, B. T. Wagaye, *et al.*, "Three-Dimensional Multilayer Vertical Filament Meshes for Enhancing Efficiency in Fog Water Harvesting," *ACS omega*, vol. 6, pp. 3910-3920, 2021.
- [126] S. Srinivasan, W. Choi, K.-C. Park, S. S. Chhatre, R. E. Cohen, and G. H. McKinley, "Drag reduction for viscous laminar flow on spray-coated non-wetting surfaces," *Soft Matter*, vol. 9, pp. 5691-5702, 2013.
- [127] M. Amrei, D. Venkateshan, N. D'Souza, J. Atulasimha, and H. V. Tafreshi, "Novel approach to measuring the droplet detachment force from fibers," *Langmuir*, vol. 32, pp. 13333-13339, 2016.
- [128] S. H. Lee, S. Y. Yeo, P. Cools, and R. Morent, "Plasma polymerization onto nonwoven polyethylene/polypropylene fibers for laccase immobilization as dye decolorization filter media," *Textile Research Journal*, vol. 89, pp. 3578-3590, 2019.
- [129] K. Kawasaki, "Study of wettability of polymers by sliding of water drop," *Journal of Colloid Science*, vol. 15, pp. 402-407, 1960.
- [130] C. Furmidge, "Studies at phase interfaces. I. The sliding of liquid drops on solid surfaces and a theory for spray retention," *Journal of colloid science*, vol. 17, pp. 309-324, 1962.
- [131] H. B. Eral, J. de Ruiter, R. de Ruiter, J. M. Oh, C. Semprebon, M. Brinkmann, *et al.*, "Drops on functional fibers: from barrels to clamshells and back," *Soft Matter*, vol. 7, pp. 5138-5143, 2011.
- [132] R. T.-P. Chow, "On the ability of drops or bubbles to stick to non-horizontal surfaces of solids," *Journal of Fluid Mechanics*, vol. 137, pp. 1-29, 1983.

9. List of publications by the author

9.1. Publications in journals

- [1] M. Azeem, A. Guérin, T. Dumais, L. Camino, R. E. Goldstein, A. I. Pesci, J. D. Rivera, *et al.*, Optimal Design of Multilayer Fog Collectors. *ACS Applied Materials & Interfaces*, vol. 12, pp. 7736-7743, 2020.
- [2] M. Azeem, J. Wiener, M. T. Noman, M. Petru, P. Louda. Structural Design of Efficient Fog Collector: A Review. *Environmental Technology and Innovation*, pp. 101169. 2020.
- [3] M. Azeem, A. Javed, M. Q. Khan, M. T. Noman, M. Shahid, J. Wiener J. Hydrophillization of Polyester Textiles by Non-Thermal Plasma. *AUTEX Research Journal*, vol. 21, pp. 142-149, 2021.
- [4] M. Azeem, A. Boughattas, J. Wiener, A. Havelka, Liquid Water Transport mechanism in fabric; A Review. *Vlakna a textil*, vol. 24, pp. 58-67, 2017
- [5] M. Azeem, M. T. Noman, M. Petru, M. Shahid, M. Q. Khan, J. Wiener, Surface wettability of vertical harps for fog collection. *Advances in Water Resources*, *Under Review*, 2021.
- [6] M. Azeem, Z. Ahmad, J. Wiener, H. F. Siddique, A. Fraz, A. Havelka, Influence of Weave Design and Yarn Types on Mechanical and Surface Properties of Woven Fabric. *FIBRES & TEXTILES in Eastern Eurpe*, vol. 26, pp. 34-37, 2018.
- [7] M. Azeem, A. Boughattas, H. F. Siddique, A. Havelka, S. Hussain, Comfort Properties of Nano-Filament Polyester Fabrics: Sensory Evaluation. *Industria Textila*, vol. 69, pp. 3-10, 2018.
- [8] M. Azeem, L. Hes, J. Wiener, M. T. Noman, A. Ali, T. Mansoor. Comfort Properties of Nano-Filament Polyester Fabrics: Thermo-physiological Evaluation. *Industria Textila*, vol. 69, pp. 315-321, 2018.
- [9] M. Azeem, J. Wiener, M. Z. Khan, Hydrophobic analysis of Nano-Filament Polyester Fabric, *Vlakna a textil*, vol. 25, pp. 8-12, 2018.
- [10] M. Azeem, A. Fraz, A. Javed, Effect of Dyeing Temperature on the Shrinkage and Fastness Properties of Polyester/Acrylic Fabric, *Pakistan Journal of Science and Research, Series A: Physical Sciences*, vol. 61A, pp. 100-105. 2018
- [11] A. Boughattas, S. Benltoufa, L. Hes, M. Azeem, F. Fayala, Thermo-physiological properties of woven structures in wet state, *Industria Textila*, vol. 69, pp. 298-303, 2018

- [12] H. F. Siddique, A. A. Mazari, A. Havelka, T. Mansoor, A. Ali, M. Azeem, Development of V-shaped compression socks on conventional socks knitting machine, *AUTEX Research Journal*. Vol. 18, pp. 377-384, 2018.
- [13] A. Boughattas, S. Benltoufa, M. Azeem, L. Hes, F. Fayala, Thermo-physiological Comfort of Brushed Woven Fabrics. *Vlakna a textil*. Vol. 25, pp. 7-12, 2018.
- [14] M. Z. Khan, S. Hussain, H. F. Siddique, V. Baheti, J. Militky, M. Azeem, A. Ali, Improvement of Liquid Moisture Management in Plaited Knitted Fabrics, *Tekstil ve Konfeksiyon*, vol. 28, pp. 182-188, 2018.
- [15] M. T. Noman, J. Militky, J. Wiener, J. Saskova, M. A. Ashraf, H. Jamshaid, M. Azeem, Sonochemical synthesis of highly crystalline photocatalyst for industrial applications, *Ultrasonics*, vol. 83, pp. 203-213, 2018.
- [16] M. T. Noman, M. Petru, J. Militky, M. Azeem, M. A. Ashraf, One-Pot Sonochemical Synthesis of ZnO Nanoparticles for Photocatalytic Applications, Modelling and Optimization. *Materials*, vol. 13, pp. 1-19, 2019.
- [17] A. Javed, M. Azeem, J. Wiener, M. Thukkaram, J. Saskova, T. Mansoor, Ultrasonically Assisted In Situ Deposition of ZnO Nano Particles on Cotton Fabrics for Multifunctional Textiles. *Fibers and Polymers*, vol. 22, pp. 77-86, 2021.
- [18] A. Salam A, M. Q. Khan, T. Hassan, N. Hassan, A. Nazir, T. Hussain, M. Azeem, I. S. Kim, In-vitro assessment of appropriate hydrophilic scaffolds by co-electrospinning of poly(1,4-cyclohexane isosorbide terephthalate)/polyvinyl alcohol, *Scientific Reports*, vol. 10, pp. 1-8, 2020.

9.2. International Conferences

- [1] M. Azeem, J. Wiener, M. K. Khan, A. Havelka, M. Shahid, Hydrophobic Treatment of Nanofilament Polyester Fabric, *9th Central European Conference*, Liberec, Czech Republic. 2017.
- [2] M. Azeem, B. Tomkova, L. Hes, J. Wiener, A. Ali, Thermal and Tactile Comfort of Nanofilament Fabric. *The 91st Textile Institute World Conference*. Leeds, UK. 2018
- [3] M. Azeem, A. Javed, J. Wiener, Hydrophilization of PET using DBD plasma, *Twenty-second international conference on composite materials (ICCM22)*. Melbourne, Australia. 2019.
- [4] A. Ali, B. Tomkova, V. Baheti, J. Militky, M. Azeem, Study the functional properties of silver nanoparticles coated fabric, *The 91st Textile Institute World Conference*, Leeds UK. 2018.

9.3. Citations

[1] M. Azeem, A. Guérin, T. Dumais, L. Camino, R. E. Goldstein, A. I. Pesci, J. D. Rivera, *et al.*, Optimal Design of Multilayer Fog Collectors. *ACS Applied Materials & Interfaces*, vol. 12, pp. 7736-7743, 2020.

- Cited in 12 articles

[2] M. Azeem, J. Wiener, M. T. Noman, M. Petru, P. Louda. Structural Design of Efficient Fog Collector: A Review. *Environmental Technology and Innovation*, pp, 101169. 2020.

- Cited in 10 articles

[3] M. Azeem, A. Boughattas, J. Wiener, A. Havelka, Liquid Water Transport mechanism in fabric; A Review. *Vlakna a textil*, vol. 24, pp. 58-67, 2017.

- Cited in 16 articles

Curriculum Vitae

Personal information	
First name / Surname	Musaddaq Azeem
Address	17 Listopadu 584, 460 15 Liberec, Liberec XV Stary Harcov. Czechia.
Mobile	+420 775 314 882
E-mail(s)	musaddaqazeem@yahoo.com musaddaq.azeem@tul.cz
Nationality	Pakistani
Place and Date of birth	Toba Tek Singh (Pakistan) on 2 th Nov 1986
Status and Gender	Married; Male
Work Experience	
Dates	06/2013 to 01/2014
Occupation or position held	Asst. Weaving Manager (Warping, Sizing, Weaving, Quality Control) SHAHRAJ Fabrics (Pvt.) Ltd, Lahore, Pakistan
Dates	2/2010 to 10/2010
Position	Officer (Commercial production & planning control), Masood Textile Mills Limited, Faisalabad, Pakistan
Education and Training	
	12/2015 - till now
Title/ Qualification	Ph.D. (Textile Engineering)
Thesis topic	<i>Scientific Design of Multilayer Fog Collectors</i>
University	Technical University of Liberec, Faculty of Textile Engineering, Department of Material Engineering
	01/2011 - 03/2013

Title/ Qualification	MS Textiles (Master)
Thesis topic	<i>Technical factors affecting the quality on the projectile weaving with Open End and Ring spun yarn</i>
University	University of Management and Technology (UMT), Lahore, PAKISTAN
	09/2006 - 03/2010
Title /Qualification	MSc (MASTER’S Fiber Technology)
Thesis topic	<i>Technological studies on dyeing behavior of acrylic fabric and its blend with polyester</i>
University	University of Agriculture, Faisalabad (UAF), Faculty of Agriculture Engineering, Department of Fiber & Textile Technology.
Internships	National Textile University, Pakistan (2016) Shinshu University, Ueda City, Japan (2017) Ghent University, Belgium (2018) Drexel University, Philadelphia, USA (2018) Adolfo Ibáñez University - Campus Viña del Mar (2018, and 2019)
Phd Supervisor	prof. Ing. Jakub Wiener , Ph.D.